2021-01-15

Ocean surface and bottom water conditions, iceberg drift and sediment transport on the North Iceland margin during MIS 3 and MIS 2

Andrews, JT

10.1016/j.quascirev.2020.106722
Quaternary Science Reviews: the international multidisciplinary research and review journal
Elsevier

Ocean surface and bottom water conditions, iceberg drift and sediment transport on the North Iceland margin during MIS 3 and MIS 2

Andrews, J.T. [1], Smik, L.[2], Belt, S.T.[2], Sicre, M-A[3], McCave, I. N.[4]

1. Institute of Arctic and Alpine Research, and Department of Geological Sciences, University of Colorado, Boulder, CO 80303
2. Biogeochemistry Research Centre, School of Geography, Earth and Environmental Sciences, University of Plymouth, Drake Circus, Plymouth, PL4 8AA, UK.
3. LOCEAN, CNRS, Sorbonne Université, Campus Pierre et Marie Curie, 4 place Jussieu, Paris, France.
4. Godwin Laboratory for Palaeoclimate Research, Department of Earth Sciences, University of Cambridge, Downing Street, Cambridge CB2 3EQ, U.K.

Orcid: Andrews: 0000-0003-3169-5979

Orcid: Belt: 0000-0002-1570-2924

Orcid: Sicre: 0000-0002-5015-1400

Orcid; McCave: 0000-0002-4702-5489

andrewsj@colorado.edu

Key words: Iceland Plateau, MIS 2 and 3, sea ice biomarkers, IP_{25}, alkenones, sortable silt, sediment provenance

Abstract

Radiocarbon dates and marine tephra suggest that the upper 10 m of core MD99-2274, off North Iceland, extends from ~0 to ~65 ka BP. A multi-proxy sediment and biomarker study at a millennial-scale resolution is used to derive a paleoclimate scenario for this area of the southwestern Nordic Seas, which during the Holocene had intermittent excursions of icebergs and a seasonal cover of drifting sea ice across the site. The sortable silt mean size ($\overline{SS}$) suggests a bottom current (1000 m depth) flow speed maximum to minimum range of ~8 cm/s during Marine Isotope Stages 2 to 3, but the data are unreliable for the Holocene. Slow-down in flow speeds may be associated with massive ice and water discharges linked to the Hudson Strait ice stream (H-events) and to melt of icebergs from Greenland in the Nordic seas where convection would have been suppressed. Five pulses of sediment with a distinct felsic component are associated with iceberg transport from E/NE Greenland. Sea ice, open water and sea surface temperature (SST) biomarker proxies (i.e. IP_{25}, HBI III, brassicasterol and alkenones) all point towards near-perennial sea ice cover during MIS 3 and 2, rather than seasonal sea ice or open water conditions. Indeed, our biomarker and sediment data require that the seas north of Iceland experienced a nearly continuous cover of sea ice, together with icebergs calved from ice stream termini, which drifted southward. The cross-correlation of the quartz % records between MD99-2274 and the well-dated core PS2644 in Blosseville Basin indicates significant coherence in the records at a multi-millennial (~8 ky) timescale. A transition to open ocean conditions is evident from the early Holocene onwards, albeit with the occurrence of some drift ice and icebergs.

1. Introduction

1.1 Aims of study

In order to gain some understanding of the complex marine environments that prevailed during the Late Quaternary we need to employ a multi-proxy approach that not only characterizes ocean surface and bottom water conditions, but also provides direct measurement of glacial influences on sediment supply. Several studies have been reported from the North Iceland Shelf (Fig. 1) that document late glacial/Holocene records (e.g. Andrews et al., 2018; McCave and Andrews, 2019a & b; Sicre et al., 2008; Knudsen et al., 2003) but there are only limited references to conditions during Marine Isotope Stages (MIS) 2, 3 or 4. Therefore, with the primary goal of establishing a framework for environmental conditions in this sector of the Iceland Sea from MIS 2 to MIS 4, we selected a previously unstudied core, MD99-2274 (Labeyrie et al., 2003) (Fig. 1), and sampled the upper 10 m. MD99-2274 (henceforth #2274) is a 10-cm diameter 26 m Calypso core retrieved from 67.582°N and 17.073°W at 1000 m water depth (Labeyrie et al., 2003) during the IMAGES V cruise aboard the French RV *Marion Dufresne*. For further context, we note that the core site is located 200 km east of the well-studied core PS2644 (van Kreveld et al., 2000; Voelker, 1999; Voelker and Haflidason, 2015) and 163 km from core P57-7 (Sejrup et al., 1989) (Table 1, Fig. 1A). The main questions we posed were: 1) what is an appropriate depth/age model, 2) is there evidence for either pervasive sea ice or an ice shelf (Boers et al., 2018; Dokken et al., 2013; Petersen et al., 2013), which have been called for to explain D-O cycles, 3) what were sea surface temperatures (SSTs), and 4) are there substantial changes in grain-size and mineral composition that can be associated with changes in bottom current flow speed and

changes in glacial sediment provenance? Given the location of the core (Fig. 1A) we were particularly interested in whether we could discriminate between glacial sediments derived from Iceland versus those from E/NE Greenland.

1.2 Present-day oceanography

The Iceland and Greenland Seas (Fig. 1A) are key areas for the formation of dense overflow waters (Brakstad et al., 2019) that flow south through sills in the ScotlandGreenland Ridge (Fig. 1C). The North Icelandic Jet (NIJ) flows southwestward along the slope below ~1000 m (Fig. 1C) with a mean speed of 9.3 m ± 2.7m/sec towards Denmark Strait (Mauritzen, 1996; Pickart et al., 2005) where it exits to form a major component of North Atlantic Deep Water *“….and points to the Iceland Sea as an important place for this water mass formation.”* (Jonsson and Valdimarsson, 2004). The study site lies in a sensitive area with the surface flow being the East Icelandic Current (EIC), which brings cold and relatively fresh surface water as a spin-off from the East Greenland Current (EGC), whereas the North Icelandic Irminger Current (NIIC), sourced from the southern warmer and saltier waters of the North Atlantic Drift (Stefansson, 1962), continues as an eastward flow over the inner North Iceland Shelf (NIC) (Fig. 1C).

Sea ice in the form of drift ice has been noted to reach the area in modern times, although the average position of the sea ice edge (30% sea ice cover by area) lies north of our site (Divine and Dick, 2006) (Fig. 1C). Thirty years of observations on the presence of icebergs (Andrews et al., 2019), their Fig. 7A) indicate that icebergs from E/NE Greenland drift across the site.

1.3 Background to study region

Stein and colleagues (Nam et al., 1995; Stein, 2008; Stein et al., 1996) studied a comprehensive suite of cores on the Scoresby Sund Trough Mouth Fan (Fig. 1A, TMF) and reported both ice-rafted debris (IRD) and $\delta^{18}O$ on the near-surface planktonic foraminifera *Neoglobquadrina pachyderma* (Table 1). The cores included discrete IRD peaks (counts 10 cm^3 > 500 µm), which they suggested may have been coeval with the massive ice and water discharges of the Hudson Strait Heinrich (HS H-) events (Andrews and Voelker, 2018b; Heinrich, 1988; Hemming, 2004; Hesse 2016). However, whether the response of the Greenland, Iceland, and European ice sheets was synchronous or asynchronous with the Laurentide Ice Sheet collapse events still requires clarification (Dowdeswell et al., 1999; Elliot et al., 2001). Verplanck et al (2009) provided radiogenic isotope data fingerprinting sediment sources from two cores on the Scoresby Sund TMF (O'Cofaigh et al., 2002) (JR51-GC31 and -GC32) and another core (PS62/017-4) from the Blosseville Basin (Milo et al., 2005) (Table 1). Stein et al. (1996) and Verplanck et al. (2009) described events in cores PS1730 and PS62/017-4 (Table 1, Fig. 1) that they considered coeval with the HS H-events. Andrews and Voelker (2018) have argued that the use of the term “Heinrich events” for locations such as the Nordic Seas is not appropriate and should be modified. For example, the IRD-rich layer in PS2644 correlated with HS H-2 (Voelker et al., 1998) is now referred to as PS2644 IRD#2 (Andrews and Voelker, 2018). In our study, events that might correlate with HS H-events will be termed #2274-IRD#.

There is no firm agreement on the extent and duration of sea ice cover in the

Nordic Seas during MIS 2 and MIS 3. The CLIMAP data showed an extensive cover across the Nordic Seas (Ruddiman and McIntyre, 1981) whereas Sarnthein et al. (2003) argue that the Nordic Seas during MIS 2 were “..largely ice free” during the summer months. The presence of an ice shelf buttressing the East Greenland ice streams has also triggered a debate especially as to a possible answer to the cause of D-O oscillations (Pettersen et al., 2013; van Kreveld et al., 2000). However, other researchers working at sites in the eastern Nordic Seas have rather focused on the role of sea ice (Dokken et al., 2013; Hoff et al., 2016) and changes in the structure of the water column, and concluded that during Greenland interstadials in MIS 3, sea ice was limited in extent and duration.

The presence of thick, pervasive sea ice could potentially limit the export of icebergs from E and NE Greenland Ice Streams (Reeh et al., 1999), although the sediment records from numerous sediment cores retrieved from the floor of the Arctic Ocean clearly document that iceberg rafting occurred throughout the Pleistocene (Clark, 1990a,b; Stein, 2008; Phillips and Grantz, 2001; Stokes et al., 2005), with some evidence that the timing of events in some cores were similar to those for HS H-events. For example, IRD peaks in cores from the Arctic Ocean were linked to the McClure Ice Stream in the NW sector of the Laurentide Ice Sheet and dated at 12.9, 15.6, ~22, and 30 ka BP (Stokes et al., 2005). Iceberg drift is primarily a function of the integrated current direction and speed over depth, plus a component associated with wind forcing on the exposed “sail” (Bigg, 2016). In many ways, sea ice protects icebergs as it inhibits wave action, which is the greatest cause of iceberg disintegration (Bigg, 2016; Venkatesh et al., 1994).

1.4 Ice sheet extent MIS 1 to MIS 3

#2274 lies only 60 km north of the LGM limit of the Iceland Ice Sheet (IIS) (Fig. 1) (Andrews and Helgadottir, 2003; Patton et al., 2017) with the onset of retreat associated with calibrated radiocarbon dates of between 14 and 15 ka BP, depending on the ocean reservoir correction (Andrews et al., 2018; Andrews and Helgadottir, 2003; Knudsen et al., 2003). Retreat from the maximum position was rapid (Andrews et al., 2018; Norðdahl and Ingolfsson, 2015; Patton et al., 2017), and the ice sheet was at or behind the presentday coast by the time of the deposition of the Vedde tephra ~12.2 ka BP (Lohne et al., 2013). Little detail is known about the history of this ice sheet during MIS 3 (e.g. Andrews et al., 2017). Moles et al. (2019) argued that the North Atlantic Ash Zone II (NAAZII) tephra, dated ca 54 ka BP (Austin and Hibbert, 2012), was erupted under >400 m of ice, thus indicating a reasonably extensive IIS during the Greenland ^{18}O stadial 15.2 (Moles et al., 2019; Rasmussen et al., 2014), but no specific information is currently available on the MIS 3 history of the ice sheet.

The Greenland Ice Sheet (GIS) extended to the shelf break during the LGM (Funder et al., 2011b; Vasskog et al., 2015) but little is known about its history during MIS 3 or MIS 4. Judging from the delivery of quartz-rich sediments to cores along Denmark Strait, especially PS2644 and MD99-2323 (Andrews and Vogt, 2020a), it is probable that the ice also reached a similar position at these times. Peterson et al. (2013) suggested that an ice shelf may have extended out from the East Greenland Shelf across Blosseville Basin, although the sedimentary evidence for this is scanty (Andrews and Vogt, 2020a).

168 *1.5 Bedrock Geology and source signatures*

169 In terms of the mineral composition of #2274 sediments, the bedrock in glacial source
170 areas consists primarily of either mafic (basalt) or felsic (granites/gneisses/sandstones),
171 although finer source identification is possible (Andrews and Vogt, 2014; 2020) (Fig.
172 1A). Further, Andrews and Vogt (2014) demonstrated that the sediment mineral
173 signature of sediments offshore from the Caledonian Fold Belt was dominated by high
174 wt% of quartz, illite, and muscovite. Detrital carbonate sediments derived from the
175 Paleozoic outcrops of N Greenland and the Canadian Arctic are also recognized by color
176 and mineralogy. However, radiogenic isotopes (White et al., 2016; Verplanck et al.,
177 2009) allow more age-related differentiations, which in terms of our region (Fig. 1A and
178 B), consists of Archaean, Paleoproterozoic, Caledonian Fold Belt, and Tertiary volcanics
179 (Henriksen, 2008).

180 **2. Environmental proxies and age model**

181 *2.1 Data methods*
182
183 The proxies used in this paper are the sea ice biomarkers IP_{25} and HBI II (Belt et al.,
184 2007; Belt and Müller, 2013; Belt, 2018), brassicasterol and HBI III as indicators of open
185 water primary production (Volkman, 1986; Belt et al., 2015), alkenones (for SST) (Sicre
186 et al., 2008a), % C37:4 alkenone to identify polar surface waters, grain-size indicators of
187 bottom flow and deposition (McCave and Andrews, 2019a, b; McCave et al., 2017),
188 magnetic susceptibility, and quantitative X-ray diffraction estimates of mineral wt%
189 (Andrews et al., 2017; Andrews and Vogt, 2014). The X-ray diffraction data for #2274
190 are available (Andrews and Vogt, 2020b) The full details of these methods are included
191 as Supplementary Material.

192
193 *2.2 Depth/age model*

194 The age model is based on radiocarbon dates and the occurrence of tephras (Table 2).
195 There are significant problems associated with obtaining and interpreting calibrated ages
196 because of the uncertainty of the ocean reservoir correction (ORC), which has varied
197 spatially and temporally, and might be as much as 1000 yr (Andrews et al., 2018; Skinner
198 et al., 2019; Voelker, 1999; Voelker et al., 1998). Three radiocarbon dates were obtained
199 on the near-surface planktonic foraminifera *Neogloboquadrina pachyderma* and the other
200 on lustrous shell fragments. Most tephras older than the Borrobol (ca 14.5 ka BP) (Lind et
201 al., 2016; Matthews et al., 2011) are dated by reference to GIS cores, which themselves
202 are based on a variety of assumptions and whose error increases with the estimated age
203 (Boers et al., 2017). The qXRD data (Andrews et al., 2013; 2018) suggest the presence of
204 high wt% of volcanic glass in two cores on the Iceland Shelf that might be coeval with
205 the Vedde and NAAZII tephras (Brendryen et al., 2011; Lohne et al., 2013). The tephra
206 bed at 607 cm in #2274 was identified by Haflidasson (person. commun. 2018) as being
207 similar to FMAZ IV dated at ~47.12 ka BP (Davies et al., 2008; Rasmussen et al., 2003;
208 Voelker and Haflidason, 2015) and that date is used in our depth/age models (see
209 Supplementary Material). Other discrete layers of black basaltic glass were noted in the
210 shipboard log at 99, 127.5, 717, and 740 cm (Labeyrie et al., 2003, p 477), and age
211 estimates were obtained from our depth/age model (see later).

212 We used the Bayesian radiocarbon calibration program “Bacon” (Blaauw and
213 Christen, 2005) to construct depth/age models, but we also acknowledge the many
214 problems associated with establishing accurate depth/age models (Telford et al., 2003;
215 Trachsel and Telford, 2017). The first model is based solely on the available ^{14}C dates and

the 607 cm tephra (Table 2A and B), while the second one is based on an assumed age estimate for the core top of 500 ± 500 (i.e. little sediment loss) and the inferred presence of the Vedde and NAAZII tephras. Given the uncertainty in the OCR, we used a ΔR = 0. In practice, there is relatively little difference in the median age estimates (Fig. 2A). The average sediment accumulation rate (SAR) is 68 yr/cm or 14.7 cm/ky, thus our 10 cm sampling density permits millennial-scale evaluations, with an average spacing between samples of 0.5 cal ky. Remarkably, for MD cores of this vintage (1999), the upper part of the core shows no evidence of piston-induced stretching (Skinner and McCave, 2003). However, the spread between minimum and maximum age estimates is often considerable given the relative paucity of dated levels, and the Bayesian approach results in an age estimate for the core top of 3600 yr BP, although the estimated date of 500 ± 500 yr BP finds some support in our data. The estimated ages for the logged tephra layers are: ~11, 13.2, 53, and 56 ka BP. A possible age for the 99 cm basaltic tephra is the 10.2 ka BP Saksunarvatn tephra (Lohne et al., 2013), which is widespread on the north Iceland Shelf (Krisjansdottir et al., 2007; Eiriksson and Knudson, 2002). All our subsequent data have been converted to a common depth/age model using the data in Table 2B; thus, robust inter-proxy comparisons can be made. To ensure that we have not forced our data into an existing framework we have not tuned our model to other records (Blaauw, 2012).

We have also obtained radiocarbon dates on several *Vema* cores that were taken to the north of Iceland and #2274 (Fig. 1; Table 3) (Manley and Jennings, 1996). The calibrated radiocarbon dates range from ~13 to > 49 ka BP (ΔR = 0) and were obtained on relatively large samples of *N. pachyderma* (Table 3). Several tephras were noted in the

core description (Suppl. Data), thus indicating that conditions allowed for the deposition of discrete tephras. The dates from these cores also provide additional information on the presence of significant numbers of the planktonic foraminifera *N. pachyderma* (Greco et al., 2019) and hence inferences about sea ice cover and light conditions.

3. Results

3.1 Lithology and Grain-size

The core log of core #2274 (Labeyrie et al., 2003. p. 477) described the sediment as being principally mottled silty clay with colors ranging between 2.5Y4/2 to 5Y4/1. Visible ice-rafted clasts occur but are not common. The grain-size measurements were undertaken on sample splits from the qXRD samples and only 30 samples were processed, resulting in a coarse resolution data set (on average one sample every 2300 yr). The sediments vary between a very coarse to a fine silt with average grain-sizes varying between 54.3 to 6.05 µm. Sand > 240 µm is considered to be ice-rafted (McCave and Andrews, 2019a) and occurs in low % throughout the core, except for two notably coarser intervals with IRD240 > 5%, (Fig. 3).

We have also undertaken an analysis of the sortable silt mean size ($\overline{SS}$) and SS% in the 63-10 µm fractions (McCave et al., 1995). The correlation coefficient between these two variables is r = 0.804 indicating, relative to other cores (McCave and Andrews, 2019a,b), a somewhat noisy correlation, but a generally current-sorted signal (Supplementary Fig. 1). Computation of the running correlation between SS% and $\overline{SS}$ yields high average values (r >0.9) between ~11 and 42 ka BP but values unacceptable for flow speed inference occur in the Holocene and during brief interval ~57 ka BP (Fig. 3). Variations in the flow speed of bottom currents (Fig. 1C) in this region reflect

changes in the vigour of the ocean overturning system because the NIJ feeds into the Denmark Strait overflow, a key starting point for the North Atlantic western Boundary Undercurrent.

The overall range (minimum-maximum) in flow speed indicated by this record is ~8 cm/s. Calibration of the sortable silt proxy yields a sensitivity (cm s^{-1}/μm) rather than an absolute speed-size relationship (McCave et al., 2017). In favourable circumstances actual speeds may be estimated by matching core-top $\overline{SS}$ data to nearby current meter measurements and plotting the differences downcore. Unfortunately, because the Holocene data are unreliable as a speed record, we cannot relate this to the present nearby flow speed measurements of 9.3 cm/sec (Jonsson, 2004). Nevertheless, low speeds correspond to HS H 1 (~15 ka), 4 (~40 ka), and 6 (~60 ka) (Fig. 3) as expected from previous work on the impact of Heinrich and other cold events on N. Atlantic circulation (e.g. Kleiven et al., 2011), on the basis of which, speeds of <5 cm/s are probable.

3.2 Mineral composition

On Figure 4, we plot the changes in the weight % of key minerals as determined by qXRD as well as the ratio quartz/pyroxene, which we use as a measure of felsic/mafic bedrock (as opposed to quartz/plagioclase which was used by Moros et al. (2004)). The quartz wt% in a surface grab from this site is ~5% (Andrews and Eberl, 2007), and the median for the whole record is 5.3 % with a maximum of 16.8 %. The magnetic susceptibility record for #2274 (Fig. 2A) is clearly inversely associated with the variations in quartz (Fig. 2B), which, together with the K-feldspars, are diamagnetic minerals (Robinson et al., 1995; Watkins and Maher, 2003). A similar inverse

relationship was noted in other cores from the area (Andrews and Vogt, 2020a). Hence the magnetic susceptibility fluctuations support our interpretation that there are substantial variations in the inputs of felsic- versus mafic-rich sediments.

The Holocene record mimics that from many sites on the North Icelandic Shelf (NIS) in showing an increase in quartz toward the present-day (Andrews et al., 2019). Quartz and pyroxene have an antiphase relationship ($r^2 = 0.47$), which in part is related to the mineral data summing to 100% (i.e. a closed array), and which provides some constraints on the interpretation (Aitchison, 1986; Chayes, 1971). There are five sustained peaks in the quartz wt % (Fig. 4), and K-feldspar (not shown, K-feldspar values track those of quartz (Andrews and Vogt, 2020a)) are therefore not included in this figure), which we interpret as indicating the influx of sediment from NE Greenland and possibly farther afield from Canada or Fennoscandia. Of these possible mechanisms, icebergs alone carry basal and englacial debris that includes all size fractions from cobbles to clay (> 1 μm). The variations in quartz are frequently matched by the sum of calcite and dolomite (carbonate) (Fig. 4) ($r^2 = 0.13$, $p < 0.0001$) although the correlations are much more significant for dolomite ($r^2 = 0.22$) than calcite ($r^2 = 0.07$). This probably represents transport of glacially derived material from the carbonate bedrock of NE and N Greenland and/or the Canadian Arctic Islands and Channels (Darby and Zimmerman, 2008; Lakeman et al., 2018; Phillips and Grantz, 2001). The estimated ages for the 5 peaks are 14.4, 31.5, 40, 54.7, and 61.8 ka BP (Fig. 4) with a possible smaller episode ~22.8 ka BP. These age estimates are somewhat similar to the HS H-events (Andrews and Voelker, 2018a; Heinrich, 1988; Hemming, 2004) (see Fig. 3) but their duration are

longer than the <1 ky episodes of detrital carbonate deposition associated with the HS Hevents (Andrews and Voelker, 2018a).

Previous work on sediment sources in this area (Verplanck et al., 2009) provide temporally limited but critical information using radiogenic isotopes on the < or > 63μm fractions. Debris flow from the two Scoresby Sund TMF sites (JR51-GC31,-32, Table 1, Fig. 1B) lay along the 1.7 Ga Paleoproterozoic isochron; the samples contained abundant quartz and lesser amounts of basalt (Verplanck et al., 2009, p.53). However, the sediments in the Blosseville Basin (core 17-4, Fig. 1A, Table 1), some 150 km downstream (Fig. 1A), and considered to be coeval with HS H events-1, -2, and -3, all cluster along the 0.5 Ga isochron (Calendonide bedrock, that outcrops on the eastern edge of NE Greenland north of Scoresby Sund (Fig. 1B)). The same isotopic signature characterized the non-HS H sediments in this core. Pb systematics indicate that the Holocene sediment samples at sites 907 (Table 1) and JR51-GC28 are dominated by the 0.5 Ga Calendonides (White et al., 2016). Given the sediment SedUnMix results (Fig. 5) and the reported radiogenic isotopic data (Verplanck et. al., 2009; White et al., 2016), the variations in quartz are most probably associated with sediment discharge events from glacial erosion and transport in ice streams flowing through the numerous fiords north of Scoresby Sund and primarily within the Caledonian Fold Belt outcrop (Evans et al., 2002, 2009; Stein, 2008).

The SedUnMix analysis included sediments from NE Greenland (Calendoides, ~73N; Andrews et al., 2016), E Greenland (basalt), and Iceland. The analysis of possible bedrock sources for the #2274 compositional changes indicated (as might be expected given the bedrock geology of E and NE Greenland, and Iceland) that the NE Greenland

source had a granite and gneissic composition, whereas E Greenland and Iceland were linked to basalt and also dolerite (Brooks and Nielsen, 1982; Henriksen, 2008; Higgins et al., 2008; Kristjansson et al., 1979). The results (Fig. 5) indicate that felsic-rich sediments from NE Greenland or farther afield (Arctic Canada, Fennoscandia) (Verplanck et al., 2009) were deposited in a series of events that mimic the influx of quartz to the site (Figs. 2B and 4); the correlation between the NE Greenland Calendonides source estimates in #2274 and the quartz wt% explains 79% of the variance. The average “unaccounted” or “unexplained” composition averaged 20 ± 5 % and degree of fit or average absolute bias is 2.3 ± 0.4 wt% indicating that the input mineral source regions provide a good fit to the #2274 mineral compositions. Figure 5 highlights two periods when the mineral composition indicates little deposition of sediment that could be ascribed to a felsic source centered around 20 and 57 ka BP, the latter being a time of substantial deposition of tephra at this site and also a time when glacial ice covered at least some of Iceland (Moles et al., 2019). Source estimates from E. Greenland (sites seaward of the early Tertiary basalt outcrop on the Geikie Plateau) and SW Iceland resulted in nearly identical patterns over the last ~65 ka BP (Fig. 5), but the results from considering Icelandic basal glacial marine diamictons (Dmm) as a source are different. The reasons for these two differing estimates are presently unclear.

The provenance time-series thus suggests that we can identify four episodes in the arrival of foreign sourced sediments; 1) from ~65 to 38 ka BP when distinct pulses of NE Greenland sourced sediments arrived; 2) 38 to 17 ka BP when there was an overall decrease in this source with virtually no quartz noted ~20 ka BP; 3) a large pulse of these sediments centered ~ 15 ka BP; and 4) the last 10 ka or so that shows a steady increase in

this source. This latter event is also noted in MD99-2269 (Fig. 7) and is matched by changes in the sea ice biomarker IP_{25} (Cabedo-Sanz et al., 2016).

3.3 Biomarkers

The sea ice biomarkers IP_{25} and HBI II were absent or below the limit of detection in the majority of the sediment sections analyzed with only a few exceptions (Fig. 6). Of the two, HBI II was always more abundant, consistent with findings from previous studies from the study region and elsewhere in the Arctic (e.g. Massé et al., 2011; Xiao et al., 2013; Bai et al., 2019). In some cases, only HBI II could be identified and quantified, with IP_{25} likely also present in such horizons but below the detection limit.

Alkenones and brassicasterol were found at very low concentrations in glacial sediments contrasting with higher abundances in Holocene sediments. Further, the open water biomarker HBI III was only detected in Holocene sediments (data not shown). While alkenone-SSTs ranged from 7 to 9°C during the Holocene, they are unexpectedly high in the glacial portion of the record, spanning from 8 to 16°C.

4. Discussion

4.1 Icebergs and IRD during MIS 3 and MIS 2

There is no general theory about the association of sea ice and icebergs and there is no observational census of the icebergs being transported in the EGC as there is for the Labrador Shelf off Newfoundland, apart from a 30-yr count of icebergs on the Iceland shelves (Jónsdóttir *in* Andrews et al., 2019). However, Cabedo-Sanz et al. (2016) and Darby et al. (2017) showed that Holocene variations in the wt% of quartz and the sea ice biomarker IP_{25} co-varied in cores to the west and south of #2274, yet this was not the case

377 at #2274 during MIS 2 and MIS 3 (Figs. 4 and 6). In N Greenland, semi-permanent
378 seaice conditions prevail today and did so intermittently during the Holocene (Funder et
379 al.,
380 2011a) and it is reasonable to assume that sea-ice would have been more extensive during
381 MIS 2 and MIS 3 when the GIS may have reached the shelf break. However,
382 cosmogenic dates pertaining to the extent of the Northeast Greenland Ice Stream at
383 ~78°N (Larsen et al., 2018) have been used to argue that this ice stream was behind its
384 present margin “…41-26 ka.”
385 Several authors have argued for the presence of an ice shelf fringing the E/NE
386 GIS (Boers et al., 2018; Petersen et al., 2013). However, sediments recovered from
387 beneath ice shelves are invariably fine-grained and lack ice-rafted debris (Domack et al.,
388 1999; Jennings et al., 2019; McKay et al., 2016), whereas the sediments from the
389 Scoresby Sund TMF (Fig. 1) and margin contain clear IRD (Stein et al., 1996) (Fig. 5; see
390 also Table 3). Radiocarbon dates in Stein et al., (1996a) were based on 2000 *N.*
391 *pachyderma* specimens per sample, and the numerous MIS 2 and MIS 3 radiocarbon
392 dates on *N. pachyderma* from PS2644 (Sarnthein et al., 2003; Voelker, 1999; Voelker et
393 al., 1998, 2000) were obtained on 10 mg samples of 800-2300 tests in 1-cm sediment
394 samples. Although the complete ecology of *N. pachyderma* is not well known, a study of
395 plankton hauls (Greco et al., 2019) indicates a relationship between sea ice cover and
396 chlorophyll, hence suggesting that *“light or light-dependent processes might influence*
397 *the ecology of this species*.” In addition, several of these cores have discrete tephra layers
398 indicating rapid accumulation of tephras by particles falling through the water column,
399 versus a more dispersed occurrence if the tephra was deposited on multi-year sea ice.

Together these data indicate that the sea ice, at times during MIS2 and 3 and probably seasonally, must have had extensive leads and open-water areas(see also Fig. 4 in Sadatzki et al., 2020).

Stein et al (1996) present detailed IRD data (counts 10 cm^3 > 500 μm) from a series of radiocarbon dated cores on the Scoresby Sund TMF (Fig. 1; PS1726 and PS1730, Fig. 1B) that reflect delivery of coarse sediments in a discrete series of episodes (data from www.Pangaea.de). Stein (2008) noted coarse sediment intervals that were attributed to iceberg-rafting at ~4-15, 16, 17-18, 20-21, and 22-23 ka BP. There are no mineral composition data for PS1730, but data exist for PS2644, which is 300 km away (Table 1, Fig. 1B) (Andrews and Vogt, 2020a; Vogt, 2017). A comparison between PS2644 and #2274 (Fig. 8A) indicates that PS2644, closer to the Scoresby Sund Ice Stream, has more quartz wt% but there are some notable corresponding peaks in both series. However, we note that the quartz wt% were obtained via two different but comparable quantitative methods (Andrews and Vogt, 2020a; Vogt, 2017; Zou, 2016). To evaluate similarities and differences between these two sites we used cross-wavelet analysis (Roesch and Schmidbauer, 2018; Hammer et al., 2001) (Fig. 8). The wavelet analysis of the two quartz records (Fig. 8A) demonstrates both important coeval events as well as obvious differences. In addition, the overall match between these sites for the earlier part of the record adds confidence to our age model, and also emphasizes the important differences between 35 and 65 ka. The reconstructed wavelets for PS2644 show three major pulses of quartz at ~13, 20, and 29 ka BP, and these are matched by much lower peaks at #2274. Conversely, there are no distinct peaks during MIS 3 in PS2644 but there are in #2274. The sense of the directional arrows in Figure 8B is that

PS2644 either leads or is in phase with #2274, and there is a hint of a significant shorter period ~60 ka BP with the two records being anti-phase. The cross-wavelet power spectrum (Fig. 8B) confirms the presence of a significant zone of coherence extending from ~10-34 ka BP with the average cross-wavelet power peaking at ~8 ky (Fig. 8C); this is of course similar to the periodicity of HS H-events (see Clark et al., 2007) (e.g. Fig. 3) but lacks the diagnostic carbonate provenance indicators (Andrews and Voelker, 2018). Possibly because of our 0.6 ky sample spacing (Fig. 8A), there is no obvious D-O signal in the quartz PS2644 data, whereas it is evident in the d ^{18}O *Np* data (Suppl. Fig. 3). The difference in signals between #2274 and PS2644 during MIS 3 (Fig. 8A) suggests a change in either the delivery of quartz-rich sediments or a dampening down of sediment delivery.

The sortable silt evidence indicates that even at the glacial maximum there was flow along the slope in the precursor to the NIJ. As this presently heads toward the Denmark Strait outflow, we suggest that the Nordic Seas acted as a source of deep waters (probably formed in the east where Atlantic inflow continued (Sarnthein et al, 1994)) that overflowed to the North Atlantic where they formed a deep water mass (Howe et al., 2016; Keigwin and Swift, 2017). The classical view of Nordic Sea behaviour during cold periods is that freshwater from melting ice-sheets and -bergs suppresses convection resulting in a severe reduction or even cessation of the AMOC inflow and overflow (e.g. a recent model, including consideration of the EGC, analysing this is from Liu et al, (2018)). However an emerging view is of a slowdown (not cessation) of Nordic Sea overflows in cold periods (Howe et al., 2016; Keigwin and Swift, 2017). A very recent view is that ice discharges in the North Pacific precede Heinrich events and may be

implicated as a triggering mechanism (Walczuk et al., 2020). In the Nordic Seas Atlantic water inflow persisted throughout the Pleistocene glacials over the Norwegian slope (Sarnthein et al., 1994; Newton et al., 2018). The evidence here indicates a persistent outflow along the N Iceland Slope with reductions during HS H- events 1, 4, and 6. Flow speed decreases have been noted for both shallow and deep flows in this region during stadials and glacial intervals of the late and mid-Quaternary (Kleiven et al., 2011; McCave and Andrews, 2019b). The Younger Dryas often shows speed decreases but some cores record increased flow (McCave and Andrews, 2019b), as is seen here. These disparities remain a puzzle.

4.2 Rationalizing mineralogical and biomarker proxies for sea ice reconstruction When detected, the concentrations of IP_{25} and HBI II were mainly much lower than those reported previously for mid-late Holocene (ca. 6-0 cal. ka) and deglacial (ca. 15-11 ka) sites from the NIS (Cabedo-Sanz et al., 2016; Xiao et al., 2017). However, the presence and concentration of IP_{25} at ca. 3.7 ka aligns with previous data reported from core JR51GC35 (located 76 km SW of #2274 (Figs.1B and 7; Table 1)) for the mid-Holocene (Cabedo-Sanz et al., 2016), consistent with the delivery of drift ice across the NIS at that time (Fig. 7). The otherwise general absence of IP_{25} and HBI II in #2274 points towards an environment unfavorable for sea ice diatom growth, namely ice-free conditions or a setting of near-permanent ice cover. To distinguish between these two scenarios, we measured three other biomarker types indicative of open water conditions, i.e. brassicasterol, HBI III and alkenones. In the case of brassicasterol, a phytosterol characteristic of marine diatoms (Volkman, 1986), concentrations in selected sediments

from #2274 were relatively high in the Holocene section and typically two orders of magnitude lower in older (>14 ka) intervals, indicative of much lower glacial primary productivity reflecting near-perennial sea ice cover. Similarly, HBI III, a biomarker derived from certain open water diatoms (Belt et al., 2017), was only detected in Holocene sections (data not shown). Consistent with these findings, concentrations of alkenones derived from coccolithophorid blooming in mid-late summers were also substantially lower in the older sections compared to those in the Holocene (Fig. 6). Further, the relatively high percentage contribution of the tetra-unsaturated alkenone $C_{37:4}$ prior to the Holocene (mean value 36% compared to 6% for the Holocene) is consistent with a dominance of polar waters (Sicre et al., 2002; Bendle et al., 2005) potentially laden with sea ice. Alkenone-derived SST estimates for the Holocene (ca. 7–9°C) are in line with those reported from other high-resolution studies from the NIS (e.g. Bendle and Rosell-Melé, 2007; Sicre et al., 2008b; Kristjansdottir et al. 2016). In contrast, SST estimates prior to the Holocene were somewhat higher (ca. 8–16°C; mean 11.4°C) although the accuracy of such estimates might be lower than for the Holocene owing to the relatively high contributions from $C_{37:4}$ (Bendle and Rosell-Melé, 2004). Anomalously warm SSTs associated with low alkenone concentrations during glacial time have been reported in previous studies and attributed to advection of detrital alkenones (Sicre et al., 2005; Knutz et al., 2011). Such advection by surface currents can introduce significant bias in regions where there are large productivity and SST gradients, thereby overprinting any local signal (Bendle and Rosell-Melé, 2004; Conte et al., 2006). With extremely low alkenone production due to the presence of ice at #2274, transport of allochthonous alkenones within the IC likely explains the deviation in SSTs

492 towards seemingly unrealistic warmer values. In any case, the most robust aspects of the
493 biomarker data
494 point towards near-perennial sea ice cover prior to the Holocene, although the presence of
495 both phytosterols and alkenones (albeit at low concentrations) indicates the occurrence of
496 at least partial open water conditions, potentially restricted to leads or regions of partial
497 ice melt within otherwise heavily consolidated pack ice. Such conditions would likely
498 have led to short-term and reduced primary production during relatively short summer
499 seasons and limited to the near-surface layer due to a strongly-stratified water column
500 resulting from partial ice melt. Both such uppermost surface layer production conditions
501 in leads and advection of allochthonous alkenones within the IC would account for the
502 anomalously high glacial SSTs.

503 Our conclusion of near-perennial sea ice during MIS 3 and MIS 2 is broadly
504 consistent with outcomes from a recent 120,000 yr reconstruction of sea-ice conditions
505 for the North Atlantic (Maffezzoli et al., 2019) based on the analysis of enriched bromine
506 (Br_{enr}) in an ice core from the Renland Ice Cap (RIC) 560 km WNW from #2274 (Figs. 1
507 and 7 [RIC]). Albeit at a much broader spatial resolution (i.e. 50-85° N), Maffezzoli et al.
508 (2019) proposed that MIS 3 and MIS 2 experienced a (variable) mix of multi-year and
509 first-year sea ice, before transitioning to mainly first-year ice and open water conditions
510 following the termination of the LGM. Interestingly, the greater range of sea ice cover
511 inferred from the RIC Br_{enr} record is not at all clear in our #2274 record, but is evident in
512 a biomarker record from the eastern Nordic Seas, with extensive/near-perennial sea ice
513 cover during stadials and H-events (i.e. comparable to #2274) but ice-free conditions

514 during interstadials (since ca. 90 ka BP); such differences between marine sites in the
515 western and eastern Nordic Seas presumably reflects the variable influence of warm
516 Atlantic water, limited to the eastern Nordic Seas (Hoff et al., 2016). Such regional
517 differences are also evident from a more recent biomarker study in the eastern Nordic Seas,
518 with significant reductions (increases) to sea ice extent during Greenland Interstadials
519 (Stadials) between ca. 41 and 32 ka (Sadatzki et al., 2020). The most prominent signature
520 of first-year ice in the Br_{enr} records occurred during the Younger Dryas and it is noteworthy
521 that a transition from permanent to increasing seasonal sea ice at the NIS was reported for
522 this interval following a biomarker-based reconstruction of surface oceanographic
523 conditions from core #2272 (Fig. 1; 7; Xiao et al., 2017). Further, based on relatively high
524 concentrations of IP_{25} in MD99-2272 during the Younger Dryas and the preceding Bølling-
525 Allerød, Xiao et al. (2017) concluded that biomarker production was likely associated with
526 locally formed first year ice rather than from advected drift ice, the latter being a feature of
527 modern-day oceanography. In contrast, our new data from #2274 indicate still near-
528 permanent sea ice cover at this time (Fig. 7). As such, we interpret the combined ice core
529 and marine sediment core data to suggest that as climate conditions ameliorated at the end
530 of the LGM, near-permanent sea ice cover transitioned to first-year seasonal sea ice in the
531 southern part of the region, especially during the Bølling-Allerød and Younger Dryas,
532 likely due to increasing influence of the IC (Xiao et al., 2017); however, the spatial extent
533 of this area of first year ice, located southward of the near-permanent sea ice front that
534 characterizes MIS 3 and MIS 2, remains uncertain at this point (see Fig. 7 sub-panel).
535 Large-scale sea ice reduction then characterized the early Holocene (Fig. 7), with a marked
536 increase in all open water primary productivity biomarker proxies (Fig. 6). Increasing drift

ice subsequently became a characteristic of the NIS from the mid Holocene onwards (Fig. 7; Cabedo-Sanz et al., 2016).

Conclusions

The multi-proxy sediment data from core #2274 130 km off the north Iceland coast appears at first sight to yield conflicting interpretations depending on whether sediment mineral composition or biomarker proxy data are being considered; however, these can be resolved through a more detailed consideration of the mode(s) of iceberg drift and trajectory through largely consolidated and near-pervasive sea ice. The low- resolution sampling for grain-size restricts detailed interpretation but the sediments are mostly moderately sorted in the silt range allowing a valid record of bottom flow speed. This shows low flow speeds during H-events 1, 4 and 6 related to decrease in Nordic Sea overflow, but not cessation, and a peak in the Younger Dryas.

The mineral composition of the < 2 mm grain-size sediment samples shows 5 peaks with wt% of quartz values significantly higher than Holocene values. The variations in the quartz wt% are also reflected in the estimated contributions of sediment from Precambrian and Caledonian bedrock sources of NE Greenland. These data require sediment transport to the #2274 site during MIS 3 and MIS 2. If the transport is by icebergs then the sea ice cover had to allow icebergs to drift southward, as they do at present (Figs. 1C, 7). A framework of near-permanent sea ice is confirmed from ultra-low seasonal sea ice and open water biomarker concentrations. On the other hand, the occurrence of non-zero concentrations of some phytoplanktic biomarkers, and numbers of near-surface planktonic foraminfera (Table 3) points to some short-term open water

559 conditions, either from limited sea ice melt or following the opening of leads; the
560 presence of drifting icebergs may be significant in this respect (Fig. 7).

561 An underlying question for HS H-events is whether North Atlantic-wide glacial
562 marine sediment events were triggered as a response to events in Hudson Strait or
563 whether the events are part of a shared response to broader regional oceanographic
564 conditions (e.g. Marcott, et al., 2011; Bassis et al., 2017; Velay-Vitow et al.,
565 2019). Thus, were "coeval" HS H- events on the East Greenland margin (Stein et al.,
566 1996; Andrews et al., 1998; Voelker, 1999), or lagged events (e.g. Baffin Bay: Simon et
567 al., 2014 Jennings et al., 2018), triggered in response to events in the Hudson Strait ice
568 stream? If our quartz and IRD events (Figs. 3 and 8) are indeed coeval with HS H-
569 events, this implies that the stability of ice streams on the NE and E Greenland shelf (and
570 N Iceland) and Hudson Strait may all have been affected by basin-wide subsurface
571 warming in response to a reduction in the Atlantic meridional overturning circulation
572 (Shaffer et al., 2004; Clark et al., 2007; Marcott et al., 2011).
573

574 **Acknowledgements**

575 We thank Dr Anne E. Jennings for picking and providing the foraminifera for the
576 radiocarbon dates, and Dr Haflidi Haflidasson for the identification and geochemical
577 analysis of the tephra. Professor Grant Bigg provided guidance on the role of icebergs
578 and sea ice. We thank the Centre National de la Recherche Scientifique (CNRS) for
579 MAS salary and the crew of the *RV* Marion Dufresne for coring operations during the
580 IMAGESV cruise. Data from this study will be archived at: www.Pangaea.de, along with
581 other IMAGESV data for MD99-2274. We acknowledge the availability and our use of

582 data from PS1726, PS1730, and PS2644, which we accessed through www.Pangaea.de.

583 Finally, we thank three anonymous reviewers who provided critical

584 and helpful feedback on previous versions of the manuscript.

585 **Tables**

586 Table 1 Location of the cores referenced in this study and showing distance from

587 MD992274. Cores located on Fig. 1A and B unless noted as NA. The last 5 sites are

588 cores that specify sediment sources based on radiogenic isotopic data (Verplanck et al.,

589 2009; White et al., 2016).

590

591 Table 2 A and B: Data for two possible depth/age models for MD99-2274 used in the

592 Bayesian "Bacon" model—see text. cc = 0 when date derived from other sources and

593 does not require calibration; cc = 2 when ocean reservoir correction DR = 0 is used

594 (marine IntelCal 13; Reimer et al., 2013).

595

596 Table 3: Depth/age data and calibrated ages for radiocarbon dates on near-surface

597 planktonic foraminifera (see Figs. 1 and 5). Ocean reservoir correction DR = 0.

598

599 **Suppl. Table:** Geochemistry of the tephra layer (see text). Courtesy Dr. H. Haflidasson)

600

601 **Figure Captions**

602 Figure 1: A) location of MD99-2274 and some other cores noted in the paper (Table 1)

603 (ODV, Schlitzer, 2011). The shaded areas represent the late glacial maximum (LGM)

604 extent of the ice sheets north of Denmark Strait; the words "basalt" and "felsic" define

605 the primary sediment mineral sources and the arrows show probable flow paths for
606 icebergs. BB = Blosseville Basi; TMF = Scoresby Sund Trough Mouth Fan; B)
607 Additional cores referenced in the paper (see also Table 1). Note that “Cald” on this
608 figure references the southern outcrop of the Greenland Caledonides (Higgins et al.,
609 2008). SS = Scoresby Sund; RIC = Renland Ice Cap. C) Surface and bottom currents and
610 historical April sea-ice edge (1870-1920) (dashed white line; Divine and Dick, 2006).
611 NIIC = North Iceland Irminger Current; EGC = East Greenland Current; EIC = East
612 Iceland Current; Yellow lines: Bottom Currents DSOW = Denmark Strait Overflow
613 Water; NIJ = North Iceland Jet., S = Separated East Greenland Current; OC = Iceland Sea
614 Ocean Convection site (after Harden et al., 2016).
615
616 Figure 2: A) Downcore plot of magnetic susceptibility (SI^{-5}) and Bayesian ((Blaauw and
617 Christen, 2016) depth age plots for MD99-2274 (see Table 2)---the red curve is for the
618 initial available data blue curve is for the estimated ages with the addition of an estimated
619 core top age and the presence of the Vedde and NAAZII tephras (see text). The Marine
620 Isotope Stage (MIS) boundaries are indicated. Location of radiocarbon dates and tephras
621 are noted. B) Plot of the departures from the median values of magnetic susceptibility
622 ($2.03 * 10^{-3}$ SI) and quartz wt% (5.3). Note that the quartz axis is reversed.
623
624 Figure 3: Variation in the Sortable Silt mean size (3-point 1-2-1 weighted smoothing with
625 raw data dots) and IRD% >240 μm. Minima in $\overline{SS}$ are seen at the time of Hudson Strait H
626 events -H6, -H4 and -H1 while -H4, -H2, early -H1 and the YD (-H0) are marked by

627 elevated IRD %. Blue bars are regions where the data are unreliable indicators of flow
628 speed according to the $\overline{SS}$ -SS% correlation criterion of McCave and Andrews, (2019a)
629
630 Figure 4: Plots of the variations in the weight% of minerals in MD99-2274, the
631 quartz/pyroxene ratio, and magnetic susceptibility. The green shaded areas represent
632 Holocene values, hence points above represent departures. Numbers 1 through 5 identify
633 IRD quartz peaks. The vertical blue shading areas represent times when the weight% of
634 quartz exceeds Holocene limits.
635
636 Figure 5: Plots of the sediment source percentages and the degree of fit (DOF), that is the
637 average absolute bias in the SedUnMix calculation of (observed mineral wt% - predicted
638 mineral weight%) for each sample. The top panel shows the location of measurable
639 quantities of gravel, and sites of tephra layers and the radiocarbon dates on near-surface
640 planktonic foraminifera (Table 3). Numbers on the NE Greenland panel represent the
641 peaks in that source and the yellow bars locate areas with minimal input from that area.
642
643 Figure 6: Biomarker data (A) IP_{25} and HBI II concentrations; (B) $\sum C_{37:3}+C_{37:2}$ alkenone
644 and brassicasterol concentrations; C) SST° C estimates and the $\%C_{37:4}$; and D) Weight %
645 quartz and different coarse sediment fractions.
646
647 Figure 7: Schematic presentation of changes in sea ice and iceberg distribution. The first
648 panel (upper left) shows core locations (see Table 1 and Fig. 1A and B) and the adjoining
649 panel the inferred conditions during MIS 3 and 2 with pervasive sea ice and embedded
650 icebergs. The remaining panels show the proposed evolution in the state of sea ice and

651 iceberg supply (red triangles) during deglaciation into the Holocene (adapted from
652 Cabedo-Sanz et al., 2016; Xiao et al., 2017). SS =Scoresby Sound, RIC=Renland Ice
653 Cap.
654
655
656 Figure 8: Analysis of the quartz wt% records from PS2644 (Vogt, 2017) and MD99-2274
657 at a common 0.6 ky spacing. A) Original quartz data (black line) and the wavelet
658 reconstructions for the two records; B) Cross-wavelet power spectrum of quartz wt% for
659 PS2644 and MD99-2274. The cone of confidence indicated by the light grey areas;
660 0.05% probability area demarcated by white line. Arrows pointing to the right mean that
661 the two records are in phase, arrows pointing down mean that x leads y, arrows pointing
662 to the left indicate the records are anti-phase and pointing up indicates that #2274 leads
663 PS2644. C) Cross-wavelet (Fig. 8B) average power. The 0.05 significance period is red
664 and delimited by the dashed slanting line. The horizontal dashed line indicates the peak
665 periodicity (~8.5 ky).
666
667
668 Suppl. Figure 1: Data for VM30-130 (see Fig. 1 and Table 3).
669
670 Suppl. Figure 2: Showing the reduced major axis association between sortable silt mean
671 size ($\overline{SS}$) and SS%.
672

Suppl. Figure 3: $\delta^{18}O$ *N. pachyderma* plots of cores from the Blosseville Basin/Scoresby Sund Trough Mouth Fan (see Fig. 1 and 8) from cores PS1730 (Stein et al., 1996a,b, and PS2644 (Voelker, 1999).

References

Aitchison, J., 1986. The statistical analysis of compositional data. Chapman and Hall, London.

Andrews, J.T., Bjork, A.A., Eberl, D.D., Jennings, A.E., Verplanck, E.P., 2015. Significant differences in late Quaternary bedrock erosion and transportation: East versus West Greenland ~ 70°N and the evolution of glacial landscapes. Journal of Quaternary Science 30, 452-463.

Andrews, J.T., Cabedo-Sanz, P., Jennings, A.E., Olafsdottir, S., Belt, S.T., Geirsdottir, A., 2018. Sea ice, ice-rafting, and ocean climate across Denmark Strait during rapid deglaciation (similar to 16-12 cal ka BP) of the Iceland and East Greenland shelves. Journal of Quaternary Science 33, 112-130.

Andrews, J.T., Cooper, T.A., Jennings, A.E., Stein, A.B., Erlenkeuser, H., 1998: Late Quaternary iceberg-rafted detritus events on the Denmark Strait–Southeast Greenland continental slope (~65°N): related to North Atlantic Heinrich events? Marine Geology 149, 211-228.

Andrews, J.T., Dunhill, G., Vogt, C., Voelker, A.H.L., 2017. Denmark Strait during the Late Glacial Maximum and Marine Isotope Stage 3: Sediment sources and transport processes. Marine Geology 390, 181-198.

Andrews, J.T., Eberl, D.D., 2007. Quantitative mineralogy of surface sediments on the Iceland shelf, and application to down-core studies of Holocene ice-rafted sediments. Journal of Sedimentary Research 77, 469-479.

Andrews, J.T., Eberl, D.D., 2012. Determination of sediment provenance by unmixing the mineralogy of source-area sediments: The "SedUnMix" program. Marine Geology 291, 24-33.

Andrews, J.T., Helgadottir, G., 2003. Late Quaternary ice cap extent and deglaciation of Hunafloaall, NorthWest Iceland: Evidence from marine cores. Arctic, Antarctic, and Alpine Research 35, 218-232.

703 Andrews, J.T., Jónsdóttir, I., Geirsdóttir, A., 2019. Tracking Holocene drift-ice limits on
704 the NW/SW Iceland shelf: comparing proxy data with observation and historical
705 evidence. Arctic, Antarctic, and Alpine Research. 51, 96-114.
706 Andrews, J.T., Kristjansdottir, G.B., Eberl, D.D., Jennings, A.E., 2013. A quantitative
707 Xray diffraction inventory of tephra and volcanic glass inputs into the Holocene
708 marine sediment archives of Iceland: A contribution to V.A.S.T. Polar Research 1-
709 15.
710 Andrews, J.T., Stein, R., Moros, M., Perner, K., 2016. Late Quaternary changes in
711 sediment composition on the NE Greenland margin (~73 degrees N) with a focus on
712 the fjords and shelf. Boreas 45, 381–397.
713 Andrews, J.T., Voelker, A., 2018. "Heinrich events" (& sediments): A history of
714 terminology and recommendations for future usage. Quaternary Science Reviews
715 187, 31-40.
716 Andrews, J.T., Vogt, C., 2014. Source to Sink: Statistical identification of regional
717 variations in the mineralogy of surface sediments in the western Nordic Seas (58°N –
718 75°N; 10° W -- 40°W). Marine Geology 357, 151-162.
719 Andrews, J.T., Vogt, C., 2020a. Variations in felsic- versus mafic-sources in the Western
720 Nordic Seas during MIS 1 to MIS 4 Marine Geology 424, 106164.
721 Andrews, J.T. and Vogt, C**.** 2020b: Results of bulk sediment X-ray diffraction analysis and
722 quantification of mineral phases based on the RockJock quantitative analysis. Pangaea.
723 https://doi.pangaea.de/10.1594/PANGAEA.923135
724 Austin, W.E.N., Hibbert, F.D., 2012. Tracing time in the ocean: a brief review of
725 chronological constraints (60-8 kyr) on North Atlantic marine event-based
726 stratigraphies. Quaternary Science Reviews 36, 28-37.
727 Bai, Y., Chen, J.F., Sicre, M.-A., Jin, H., Ren, J., Li, H., Xue, B., Ji, Z., Zhuang, Y.,
728 Klein, V., Zhao, M., 2019. Seasonal and spatial variability of sea ice and
729 phytoplankton biomarker flux in the Chukchi Sea (Western Arctic). Progress in
730 Oceanography 171, 22-37.
731 Bassis, J.N., Petersen, S.V. Cathles, L.M., 2017. Heinrich events triggered by ocean
732 forcing and modulated by isostatic adjustment. Nature 542, 332-334.

733 Belt, S.T., 2018. Source-specific biomarkers as proxies for Arctic and Antarctic sea ice,
734 Organic Geochemistry 125, 277–298, doi: 10.1016/j.orggeochem.2018.10.002.
735 Belt, S.T., Masse, G., Rowland, S.J., Poulin, M., Michel, C., LeBlanc, B., 2007. A novel
736 chemical fossil of palaeo sea ice: IP_{25}. Organic Gechemistry 38, 16-27.
737 Belt, S.T., Müller, J., 2013. The Arctic sea ice biomarker IP_{25}: a review of current
738 understanding, recommendations for future research and applications in palaeo sea
739 ice reconstructions. Quaternary Science Reviews 79, 9-25.
740
741 Belt, S.T., Cabedo-Sanz, P., Smik, L., Navarro-Rodriguez, A., Berben, S.M. P., Knies, J.,
742 Husum, K., 2015. Identification of paleo Arctic winter sea ice limits and the marginal
743 ice zone: optimised biomarker-based reconstructions of late Quaternary Arctic sea
744 ice. Earth and Planetary Science Letters 431, 127-139.
745 Belt, S.T., Brown, T.A., Smik, L., Tatarek, A., Wiktor, J., Stowasser, G., Assmy, P.,
746 Allen, C.A., Husum, K., 2017. Identification of C_{25} highly branched isoprenoid
747 (HBI) alkenes in diatoms of the genus *Rhizosolenia* in polar and non-polar marine
748 phytoplankton. Organic Geochemistry 110, 65–72
749 Bendle, J., Rosell-Melé, A., 2004. Distributions of UK'_{37} and UK_{37} in the surface waters
750 and sediments of the Nordic Seas: implications for paleoceanography. Geochemistry,
751 Geophysics, Geosystems, Q11013. doi:10.1029/2004GC000741.
752 Bigg, G.R., 2016. Icebergs. Their Science and links to Global Change. Cambridge
753 University Press.
754 Blaauw, M., 2012. Out of tune: the dangers of aligning proxy archives. Quaternary Science
755 Reviews 36, 38-49.
756 Blaauw, M., Christen, J.A., Bacon Manual, 2016. -v2.2, p. 11 pp.
757 Blaauw, M., Christen, J.A., 2005. The problems of radiocarbon dating. Science 308,
758 1552-1553.
759 Boers, N., Ghil, M., Rousseau, D.D., 2018. Ocean circulation, ice shelf, and sea ice
760 interactions explain Dansgaard-Oeschger cycles. Proceedings of the National
761 Academy of Sciences of the United States of America 115, E11005-E11014.

762 Boers, N., Goswami, B., Ghil, M., 2017. A complete representation of uncertainties in
763 layer-counted paleoclimate archives. Climate of the Past 13, doi:10.5194/cp-131169-
764 2017
765 Brakstad, A., Vage, K., Havik, L., Moore, G.W.K., 2019. Water Mass Transformation in the
766 Greenland Sea during the Period 1986-2016. Journal of Physical Oceanography 49,
767 121140.
768 Brendryen, J., Haflidason, H., Sejrup, H.P., 2011. Non-synchronous deposition of North
769 Atlantic Ash Zone II in Greenland ice cores, and North Atlantic and Norwegian Sea
770 sediments: an example of complex glacial-stage tephra transport. Journal of
771 Quaternary Science 26, 739-745.
772 Brooks, C.K., Nielsen, T.F.D., 1982. The Phanerozoic development of the
773 Kangerdlugssuaq area, East Greenland. Meddelelser on Gronland, Geoscience 9, 1-
774 30.
775 Cabedo-Sanz, P., Belt, S.T., Jennings, A.E., Andrews, J.T., Geirsdóttir, Á., 2016.
776 Variability in drift ice export from the Arctic Ocean to the North Icelandic Shelf over
777 the last 8000 years: A multi-proxy evaluation. Quaternary Science Reviews 146,
778 99115.
779 Chayes, F., 1971. Ratio correlation. University of Chicago Press, Chicago.
780 Clark, D.L., 1990a. Arctic Ocean ice cover; Geologic history and climatic significance,
781 The Geology of North America. Geological Society of America, pp. 53-62.
782 Clark, D.L., 1990b. Stability of the Arctic Ocean ice-cover and Pleistocene warming
783 events: Outlining the problem, in: Bleil, U., Thiede, J. (Eds.), Geological History of
784 the Polar Oceans: Arctic Versus Antarctic. Kluwer Academic Publishers,
785 Netherlands, pp. 273-287.
786 Clark, P. U., Hostetler, S. W., Pisias, N. G., Schmittner, A., and Meissner, K. J., 2007.
787 Mechanisms for a ~7 kyr climate and sea-level oscillation during marine isotope stage
788 3. In Schmittner, A., Chiang, J., and Hemming, S. (eds.), *Ocean Circulation:*
789 *Mechanisms and Impacts*. Geophysical Monograph 173. Washington, DC: AGU, pp.
790 209–246.
791 Conte, M. H., M.-A. Sicre, C. Rühlemann, J. C. Weber, S. Schulte, D. Schulz-Bull, T.

792 Blanz, 2006. Global temperature calibration of the alkenone unsaturation index
793 ($U^{K'}_{37}$) in surface waters and comparison with surface sediments, *Geochemistry*,
794 *Geophysics, Geosystems* **7**, Q02005, doi:10.1029/2005GC001054.
795 Darby, D.A., Andrews, J.T., Belt, S.T., Jennings, A.E., Cabedo-Sanz, P., 2017. Holocene
796 cyclic records of ice-rafted debris and sea ice variations on the East Greenland and
797 NW Iceland margins. Antarctic, Arctic, and Alpine Research 49, 649-672.
798 Darby, D.A., Zimmerman, P., 2008. Ice-rafted detritus events in the Artic during the last
799 glacial interval, and the timing of the Innuitian and Laurentide ice sheet calving
800 events. Polar Research 27, 114-127.
801 Davies, S.M., Wastegard, S., Rasmussen, T.L., Svensson, A., Johnsen, S.J., Steffensen,
802 J.P., Andersen, K.K., 2008. Identification of the Fugloyarbanki tephra in the NGRIP
803 ice core: a key tie-point for marine and ice-core sequences during the last glacial
804 peroid. Quaternary Science Reviews 23, 409-414.
805 Divine, D.V., Dick, C., 2006. Historical variability of the sea ice edge position in the
806 Nordic Seas. Journal of Geophysical Research 111, 14pp.
807 doi:10.1029/2004JC002851.
808 Dokken, T.M., Nisancioglu, K.H., Li, C., Battisti, D.S., Kissel, C., 2013.
809 DansgaardOeschger cycles: Interactions between ocean and sea ice intrinsic to the
810 Nordic seas.
811 Paleoceanography 28, 491-502.
812 Domack, E.W., Jacobson, E.A., Shipp, S., Anderson, J.B., 1999. Late
813 PleistoceneHolocene retreat of the West Antarctic Ice-Sheet system in the Ross Sea:
814 Part 2 - Sedimentologic and stratigraphic signature. Geological Society of America
815 Bulletin 111, 1517-1536.
816 Dowdeswell, J.A., Elverhoi, A., Andrews, J.T., Hebbeln, D., 1999. Asynchronous de-
817 position of ice-rafted layers in the Nordic seas and North Atlantic Ocean. Nature 400,
818 348–351.
819 Eberl, D.D., 2003. User guide to RockJock: A program for determining quantitative
820 mineralogy from X-ray diffraction data. United States Geological Survey, Open File
821 Report 03-78, 40 pp, Washington, DC.

822 Elliot, M., Labeyrie, L., Dokken, T., Manthe, S., 2001. Coherent patterns of ice-rafted
823 debris deposited in the Nordic regions during the last glacial (10-60 ka). Earth and
824 Planetary Science Letters 194, 151–163.
825 Evans, J., Dowdeswell, J. A., Grobe, H., Niessen, F., Stein, R., Hubberten, H.-W. &
826 Whittington, R. J. 2002: Late Quaternary sedimentation in Kaiser Joseph Fjord and
827 the continental margin of East Greenland. In Dowdeswell, J. A. & O Cofaigh, C.
828 (eds.): Glacier-Influenced Sedimentation on High-Latitude Continental Margins,
829 Special Publication 203, 149–179. The Geological Society of London, London.
830 Evans, J., Dowdeswell, J. A., Grobe, H., Niessen, F., Stein, R., Hub- berten,
831 H.-W. & Whittington, R. J. 2002: Late Quaternary sedi- mentation in
832 Kejser Joseph Fjord and the continental margin of East Greenland. I
833 n Dowdeswell, J. A. &O Cofaigh, C. (eds.):
834 Glacier-Influenced Sedimentation on High-Latitude Continental
835 Margins, 149–179. The Geological Society of London, Special
836 Publication 203, London.
837 Evans, J., O Cofaigh, C., Dowdeswell, J. A. & Wadhams, P. 2009:
838 Marine geophysical evidence for former expansion and flow of the
839 Greenland Ice Sheet across the north-east Greenland continental shelf.
840 Journal of Quaternary Science 24, 279–293.
841 Evans, J., Dowdeswell, J. A., Grobe, H., Niessen, F., Stein, R., Hub-
842 berten, H.-W. & Whittington, R. J. 2002: Late Quaternary sedi-
843 mentation in Kejser Joseph Fjord and the continental margin of
844 East Greenland. I n Dowdeswell, J. A. & O Cofaigh, C. (eds.):
845 Glacier-Influenced Sedimentation on High-Latitude Continental
846 Margins, 149–179. The Geological Society of London, Special
847 Publication 203, London.
848 Evans, J., O Cofaigh, C., Dowdeswell, J. A. & Wadhams, P. 2009:
849 Marine geophysical evidence for former expansion and flow of the
850 Greenland Ice Sheet across the north-east Greenland continental shelf.
851 Journal of Quaternary Science 24, 279–293.

852 Evans, J., Dowdeswell, J. A., Grobe, H., Niessen, F., Stein, R., Hubberten, H.-W. &
853 Whittington, R. J. 2002: Late Quaternary sedi- mentation in Kejser Joseph Fjord and
854 the continental margin of East Greenland. In Dowdeswell, J. A. & O Cofaigh, C.
855 (eds.): Glacier-Influenced Sedimentation on High-Latitude Continental Margins,
856 149–179. The Geological Society of London, Special Publication 203, London.
857 Evans, J., O Cofaigh, C., Dowdeswell, J. A. & Wadhams, P. 2009: Marine geophysical
858 evidence for former expansion and flow of the Greenland Ice Sheet across the
859 northeast Greenland continental shelf. Journal of Quaternary Science 24, 279–293.
860 Funder, S., Goosse, H., Jepsen, H., Kaas, E., Kjaer, K.H., Korsgaard, N.J., Larsen, N.K.,
861 Linderson, H., Lysa, A., Moller, P., Olsen, J., Willerslev, E., 2011a. A 10,000-year
862 record of Arctic Ocean sea-ice variability-view from the beach. Science, 333,
863 747750.
864 Funder, S., Kjeldsen, K.K., Kjaer, K.H., O Cofaigh, C., 2011b. The Greenland Ice Sheet
865 during the past 300,000 years: A review. p. 699-713 In, Ehlers, J., Gibbard, P.L., and
866 Hughes, P.D., (Eds), Quaternary Glaciations - Extent and Chronology: A Closer
867 Look. Elsevier, Amsterdam
868 Greco, M., Jonkers, L., Kretschmer, K., Bijma, J., Kucera, M., 2019. Depth habitat of the
869 planktonic foraminifera *Neogloboquadrina pachyderma* in the northern high latitudes
870 explained by sea-ice and chlorophyll concentrations. Biogeosciences 16, 3425-3437.
871 Hammer, O, Harper, D.A.T., and Ryan, P.D., 2001. PAST: Paleontological statistics
872 software package for education and data analysis. Palaelontological Electonica,
873 http://palaeo-electorica.org
874 Harden, B.E., Pickart, R.S., Valdimarsson, H., Vage, K., de Steur, L., Richards, C., Bahr,
875 F., Torres, D., Borve, E., Jonsson, S., Macrander, A., Osterhus, S., Havik, L.,
876 Hattermann, T., 2016. Upstream sources of the Denmark Strait Overflow:
877 Observations from a high-resolution mooring array. Deep-Sea Research Part I-
878 Oceanographic Research Papers 112, 94-112
879 Hassani, H., 2007. Singular Spectrum Analysis: Methodology and comparison. Journal of
880 Data Science 5, 239-257.
881 Heinrich, H., 1988. Origin and consequences of cyclic ice rafting in the Northeast
882 Atlantic Ocean during the past 130,000 years. Quaternary Research 29, 143-152.

883 Hemming, S.R., 2004. Heinrich Events: Massive late Pleistocene detritus layers of the
884 North Atlantic and their global climate imprint. Reviews of Geophysics 42,
885 RG1005/2004.
886 Henriksen, H., 2008. Geological history of Greenland. Geological Survey of Denmark
887 and Greenland, Copenhagen.
888 Hesse, R., 2016. Ice-proximal Labrador Sea Heinrich layers: a sedimentological
889 approach. Canadian Journal of Earth Sciences 53, 71-100.
890 Higgins, A.K., Gilotti, J.A., Smith, P.M., 2008. The Greenland Caledonides. Evolution of
891 the Northeast margin of Laurentia. Geological Society of America, Boulder, CO, p.
892 368.
893 Hoff, U., Rasmussen, T.L., Stein, R., Ezat, M.M., Fahl, K., 2016. Sea ice and
894 millennialscale climate variability in the Nordic seas 90 kyr ago to present. Nature
895 Communications 7. 12247.
896 Howe, J.N.W., Piotrowski, A.M., Noble, T.L., Mulitza, S., Chiessi, C.M., Bayon, G.,
897 2016. North Atlantic Deep Water production during the Last Glacial Maximum.
898 Nature Commun. 7, 11765. doi: 10.1038/ncomms11765
899 Jennings, A.E., Andrews, J.T. et al.., 2018. Baffin Bay paleoenvironments in the LGM
900 and HS1: Resolving the ice-shelf question. Marine Geology. 402, 5-16.
901 Jennings, A.E., Reilly, B., Andrews, J.T., Hogen, K., Walczak, M., Stoner, J., Mix, A.C.,
902 Jakobsson, M., 2019. Modern ice shelf facies and Early Holocene counterparts in
903 Petermann Fjord and Northern Nares Strait, International Association Sedimentology
904 IAS, Rome.
905 Jonsson, S., and Valdimarsson, H. 2004. A new path for the Denmark Strait overflow
906 water from the Iceland Sea to Denmark Strait. Geophysical Research Letters 31, 4pp.
907 doi:10.1029/2003GL019214, 012004.
908 Jonsson, S., Valdimarsson, H., 2005. The flow of Atlantic water to the North Icelandic
909 Shelf and its relation to the drift of cod larvae. ICES Journal of Marine Science 62,
910 1350-1359.
911 Jonsson, S., Briem, J., 2003. Flow of Atlantic water west of Iceland and onto the north
912 Atlantic shelf. ICES Marine Science Symposia 219, 326-328.

913 Keigwin, L.D.,and Swift, S.A., 2017. Carbon isotope evidence for a northern source of
914 deep water in the glacial western North Atlantic. Proceedings of the National
915 Academy of Sciences of the United States of America 114, 2831-2835.
916 Knudsen, K.-L., Eiriksson, J., 2002. Application of tephrachronology to the timing and
917 correlation of palaeoceanographic events recorded in Holocene and Late Glacial
918 shelf sediments off North Iceland. Marine Geology 191, 165-188.
919 Konert, M., Vandenberghe, J., 1997. Comparison of laser grain size analysis with pipette
920 and sieve analysis: a solution for the underestimation of the clay fraction.
921 Sedimentology 44, 523-535.
922 Knudsen, K.-L., Jiang, D., Jansen, E., Eiriksson, J., Heinemeier, J., Seidenkrantz, M.-S.,
923 2003. Environmental changes off North Iceland during the deglaciation and the
924 Holocene: foraminifera, diatoms and stable isotopes. Marine Micropaleontology 953,
925 1-33.
926 Knutz, P.C., H. Ebbesen, S. Christiansen**,** M.-A. Sicre, and A. Kuijpers, 2011. The triple
927 stage deglacial retreat of the southern Greenland Ice Sheet driven steps by vigorous
928 Irminger Current, and its significance for the Younger Dryas cooling,
929 *Paleoceanography, 26, PA3204*, doi:10.1029/2010PA002053, 2011
930 Kristjansdottir, G.B., Stoner, J.S., Gronvold, K., Andrews, J.T., Jennings, A.E., 2007.
931 Geochemistry of Holocene cryptotephras from the North Iceland Shelf (MD992269):
932 Intercalibration with radiocarbon and paleomagnetic chronostratigraphies.
933 The Holocene 17, 155-176.
934 Kristjansson, L., Saemundsson, K., Thorarinsson, S., Saemundsson, K., Thorarinsson, S.,
935 Einarsson, P., Bjornsson, S., Simonarson, L., Fridleifsson, I., Jaksobsson, S.P.,
936 Bjornsson, H., 1979. Special Issue: Geology of Iceland. Jökull 29, 1-101.
937 Labeyrie, L., Jansen, E., Cortijo, E., 2003. Les rapports de campagnes a la mer
938 MD114/IMAGES V. Institut Polaire Francais Paul-Emile Victor, Brest.
939
940 Labeyrie, L.D. and Cortijo, E. 2005: Physical properties of sediment core MD99-2274.
941 Pangaea. https://doi.org/10.1594/PANGAEA.253605

Lakeman, T.R., Pienkowski, A.J., Nixon, F.C., Furze, M.F.A., Blasco, S., Andrews, J.T., King, E.L., 2018. Collapse of a marine-based ice stream during the early Younger Dryas chronozone, western Canadian Arctic. Geology 46, 211-214.

Larsen, N.K., Levy, L.B., Carlson, A.E., Buizert, C., Olsen, J., Strunk, A., Bjork, A.A. and Skov, D.S. (2018) Instability of the Northeast Greenland Ice Stream over the last 45,000 years. *Nature Communications*, 9.doi: 10.1038/s41467-018-04312-7

Lind, E.W., Lilja, C., Wastegard, S., Pearce, N.J.G., 2016. Revisiting the Borrobol Tephra. Boreas 45, 693-643.

Liu, Y., Hallberg, R., Sergienko, O., Samuels, B.L., Harrison, M., & Oppenheimer, M. 2018. Climate response to the meltwater runoff from Greenland ice sheet: evolving sensitivity to discharging locations. Climate Dynamics, 51, 1733–1751. doi 10.1007/s00382-017-3980-7

Lohne, O.S., Mangerud, J., Birks, H.H., 2013. Precise C-14 ages of the Vedde and Saksunarvatn ashes and the Younger Dryas boundaries from western Norway and their comparison with the Greenland Ice Core (GICC05) chronology. Journal of Quaternary Science 28, 490-500.

Maffezzoli, N., Vallelonga, P., Edwards, R., Saiz-Lopez, A., Turetta, C., Kjaer, H.A., Barbante, C., Vinther, B., Spolaor, A., 2019. A 120 000-year record of sea ice in the North Atlantic? Climate of the Past 15, 2031-2051.

Manley, W.F., Jennings, A.E., 1996. Radiocarbon Date List VIII: Eastern Canadian Arctic, Labrador, Northern Quebec, East Greenland Shelf, Iceland Shelf, and Antarctica. INSTAAR, University of Colorado, p. 163 pp.

Marcott, S.A., Clark, P.U., Padman, L., Klinkhammer, G.P., Springer, S.R. , Liu, Z., , Otto-Bliesner, B.L., Carlson, A.E., Ungerer, A., Padman, J., He, F., Cheng, J. and Schmittner, A., 2011: Ice-shelf collapse from subsurface warming as a trigger for Heinrich events. Proceedings of the National Academy of Sciences of the United States of America 108, 13415-13419

Marshall, N.R., Piper, D.J.W., Saint-Ange, F., Campbell, D.C., 2014. Late Quaternary history of contourite drifts and variations in Labrador Current flow, Flemish Pass, offshore eastern Canada. Geology Marine Letters 34, 457-470. doi:10.1007/s00367014-0377-z.

973 Mauritzen, C., 1996. Production of dense overflow waters feeding the North Atlantic
974 across the Greenland-Scotland Ridge. 1. Evidence for a revised circulation scheme.
975 Deep-Sea Research I 43, 769-806.
976 Massé, G., Rowland, S.J., Sicre, M.-A., Jacob, J., Jansen, E., Belt, S.T., 2008. Abrupt
977 climate changes for Iceland during the last millennium: Evidence from high resolution
978 sea ice reconstructions. Earth and Planetary Science Letters 269, 565–569. Matthews,
979 I.P., Birks, H.H., Bourne, A.J., Brooks, S.J., Lowe, J.J., Macleod, A., PyneO'Donnell,
980 S.D.F., 2011. New age estimates and climatostratigraphic correlations for
981 the Borrobol and Penifiler Tephras: evidence from Abernethy Forest, Scotland.
982 Journal of Quaternary Science 26, 247-252.
983 McCave, I.N., Andrews, J.T., 2019a. Distinguishing current effects in sediments
984 delivered to the ocean by ice. I. Principles, methods and examples. Quaternary
985 Science Reviews 212, 92-107.
986 McCave, I.N., Andrews, J.T., 2019b. Distinguishing current effects in sediments
987 delivered to the ocean by ice. II. Glacial to Holocene changes in North Atlantic high
988 latitude upper ocean flows. Quaternary Science Reviews 223, no. 105902, 21pp.
989 McCave, I.N., Hall, I.R., Bianchi, G.G., 2006. Laser vs settling velocity differences in silt
990 grainsize measurements: estimation of palaeocurrent vigour. Sedimentology 53,
991 919928.
992 McCave, I.N., Manighetti, B. and Robinson, S.G., 1995. Sortable silt and fine sediment
993 size/composition slicing: parameters for palaeocurrent speed and palaeoceanography.
994 Paleoceanography 10, 593-610.
995 McCave, I.N., Thornalley, D.J.R., Hall, I.R., 2017. Relation of sortable silt grain-size to
996 deep-sea current speeds: Calibration of the 'Mud Current Meter'. Deep-Sea Research
997 Part I 127, 1-12.
998 McCave, I.N., Syvitski, J.P.M, 1991. Principles and methods of geological particle size
999 analysis, in: Syvitski, J.P.M. (Ed.), Principles, methods and application of particle
1000 size analysis. Cambridge University Press, pp. 3-21.
1001 McKay, R., Golledge, N.R., Maas, S., Naish, T., Levy, R., Dunbar, G., Kuhn, G., 2016.
1002 Antarctic marine ice-sheet retreat in the Ross Sea during the early Holocene.
1003 Geology 44, 7-10.

1004 Millo, C., Sarnthein, M., Erlenkeuser, H., Frederichs, T., 2005. Methane-driven Late
1005 Pleistocene delta C-13 minima and overflow reversals in the southwestern Greenland Sea.
1006 Geology 33, 873–876.
1007 Moles, J.D., McGarvie, D., Stevenson, J.A., Sherlock, S.C., Abbott, P.M., Jenner, F.E.,
1008 Halton, A.M., 2019. Widespread tephra dispersal and ignimbrite emplacement from a
1009 subglacial volcano (Torfajokull, Iceland). Geology 47, 577-580.
1010 Moros, M., McManus, J., Rasmussen, T., Kuijpers, A., Dokken, T., Snowball, I., Nielsen,
1011 T., Jansen, E., 2004. Quartz content and the quartz-to-plagioclase ratio determined
1012 by X-ray diffraction: a proxy for ice rafting in the northern North Atlantic? Earth and
1013 Planetary Science Letters 218, 389-401.
1014 Newton, A.M.W., Huuse, M., and Brocklehurst, S.H. 2018. A persistent Norwegian
1015 Atlantic Current through the Pleistocene glacials. Geophysical Research Letters 45,
1016 5599–5608. https://doi.org/10.1029/2018GL077819
1017 Nam, S.-I., Stein, R., Grobe, H., Hubberten, H., 1995. Late Quaternary glacial/interglacial
1018 changes in sediment composition at the East Greenland continental margin and their
1019 paleoceanographic implications. Marine Geology 122, 243-262.
1020 Norðdahl, H., Ingolfsson, O., 2015. Collapse of the Icelandic ice sheet controlled by
1021 sealevel rise? Arktos, 1 pp 1-18.
1022 O'Cofaigh, C., Taylor, J., Dowdeswell, J.A., Rosell-Mele, A., Kenyon, N.H., Evans, J.,
1023 Mienert, J., 2002. Geological evidence for sediment reworking on high-latitude
1024 continental margins and its implications for palaeoceanography: insights from the
1025 Norwegian– Greenland Sea. In: Dowdeswell, J.A., Ó Cofaigh, C. (Eds.),
1026 Glacierinfluenced sedimentation on high-latitude continental margins. Geological Society
1027 London Special Paper, 20. Geological Society, London, pp. 325–348.
1028 Paillard, D., Labeyrie, L., Yiou, P., 1996. Macintosh program performs time-series
1029 analysis. EOS 77, 379.
1030 Patton, H., Hubbard, A., Bradwell, T., Schomacker, A., 2017. The configuration,
1031 sensitivity and rapid retreat of the Late Weischelian Icelandic Ice Sheet.
1032 EarthScience Reviews 166, 223-245.
1033 Petersen, S.V., Schrag, D.P., Clark, P.U., 2013. A new mechanism for
1034 DansgaardOeschger cycles. Paleoceanography 28, 24-30.

1035 Phillips, R.L., Grantz, A., 2001. Regional variations in provenance and abundance of
1036 icerafted clasts in Arctic Ocean sediments: implications for the configuration of late
1037 Quaternary oceanic and atmospheric circulation in the Arctic. Marine Geology 172,
1038 91-115.
1039 Pickart, R.S., Torres, D.J., Fratantoni, P.S., 2005. the East Greenland spill jet. Journal of
1040 Physical Oceanography 35, 1037-1053.
1041 Prahl, F.G., Muelhausen, L.A., Zahnle, D.L., 1988, Further evaluation of long-chain
1042 alkenones as indicators of paleoceanographic conditions. Geochimica et
1043 Cosmochmicia Acta 52, 2303-2310.
1044 Rasmussen, S.O., Bigler, M., Blockley, S.P., Blunier, T., Buchardt, S.L., Clausen, H.B.,
1045 Cvijanovic, I., Dahl-Jensen, D., Johnsen, S.J., Fischer, H., Gkinis, V., Guillevic, M.,
1046 Hoek, W.Z., Lowe, J.J., Pedro, J.B., Popp, T., Seierstad, I.K., Steffensen, J.P.,
1047 Svensson, A.M., Vallelonga, P., Vinther, B.M., Walker, M.J.C., Wheatley, J.J.,
1048 Winstrup, M., 2014. A stratigraphic framework for abrupt climatic changes during
1049 the Last Glacial period based on three synchronized Greenland ice-core records:
1050 refining and extending the INTIMATE event stratigraphy. Quaternary Science
1051 Reviews 106, 14-28.
1052 Rasmussen, T.L., Wastegard, S., Kuijpers, A., van Weering, T.C.E., Heinemeier, J.,
1053 Thomsen, E., 2003. Stratigraphy and distribution of tephra layers in marine sediment
1054 cores from the Faeroe Islands, North Atlantic. Marine Geology 199, 263-277.
1055 Reeh, N., 2004. Holocene climate and fjord glaciations in Northeast Greenland:
1056 implications for IRD deposition in the North Atlantic. Sedimentary Geology 165,
1057 333-342.
1058 Reeh, N., Mayer, C., Miller, H., Thomsen, H.H., Weidick, A., 1999. Present and past
1059 climate control on fjord glaciations in Greenland: Implications for IRD-deposition in
1060 the sea. Geophysical Research Letters 26, 1039-1042.
1061 Reimer, P.J., Bard, E., Bayliss, A., Beck, J.W., Blackwell, P.G., Bronk Ramsey, C., Grootes,
1062 P.M., Guilderson, T.P., Haflidason, H., Hajdas, I., Hatt?, C., Heaton, T.J., Hoffmann, D.L.,
1063 Hogg, A.G., Hughen, K.A., Kaiser, K.F., Kromer, B., Manning, S.W., Niu, M., Reimer,
1064 R.W., Richards, D.A., Scott, E.M., Southon, J.R., Staff, R.A., Turney, C.S.M. and van

1065 der Plicht, J. (2013) IntCal13 and Marine13 Radiocarbon Age Calibration Curves 0-
1066 50,000 Years cal BP. *Radiocarbon*, 55, 1869-1887.
1067 Robinson, S.G., Maslin, M.A., McCave, I.N., 1995. Magnetic susceptibility variations in
1068 Upper Pleistocene deep-sea sediments of the N.E. Atlantic: Implications for ice
1069 rafting and palaeocirculation at the Last Glacial Maximum. Paleoceanography 10,
1070 221-250.
1071 Roesch, A. and Schmidbauer, H.W.C., 2018: WaveletComp: Computational Wavelet
1072 Analysis. R package 1.1. https//CRAN.R-project.org/package=Wavelet.Comp.
1073 Ruddiman, W.F., McIntyre, A., 1981. The North Atlantic Ocean during the last
1074 deglaciation. Palaeogeography, Palaeoclimatology, Palaeoecology 35, 145-214.
1075 Sadatzki, H., Maffezzoli, N., Dokken, T.M., Simon, M.H., Berben, S.M.P., Fahl, K.,
1076 Kjær, H.A., Spolaor, A., Stein, R., Vallelonga, P., Vinther, P.M., Jansen, E., 2020.
1077 Rapid reductions and millennial-scale variability in Nordic Seas sea ice cover during
1078 abrupt glacial climate changes. Proceedings of the National Academy of Sciences
1079 202005849. doi.org/10.1073/pnas.2005849117.
1080 Sarnthein, M., Winn, K., Jung, S., Duplessy, J. C., Labeyrie, L., Erlenkeuser, H., and
1081 Ganssen, G., 1994. Changes in East Atlantic deepwater circulation over the last
1082 30,000 years – An eight-time-slice record. Paleoceanography 9, 209–267.
1083 Sarnthein, M., Pflaumann, U., Weinelt, M., 2003. Past extent of sea ice in the northern
1084 North Atlantic inferred from foraminiferal paleotemperature estimates.
1085 Paleoceanography 18, doi:10.1029/2002PA000771.
1086 Schlitzer, R., 2011. Ocean Data View, http://odv.awi.de,2011.
1087
1088 Sejrup, H.P., Sioholm, J., Furnes, H., Beyer, I., Eide, L., Jansen, E., Mangerud, J., 1989.
1089 Quaternary tephrachronology on the Iceland Plateau, north of Iceland. Journal of
1090 Quaternary Science 4, 109-114.
1091 Shaffer, G., S.M. Olsen, and C.J. Bjerrum, 2004. Ocean subsurface warming as a
1092 mechanism for coupling Dansgaard-Oeschger climate cycles and ice-rafting events.
1093 Geophysical Research Letters 31, L24202, doi:10.1029/2004GL020968.

1094 Sicre, M.-A., Bard, E., Ezat, U., Rostek, F., 2002. Alkenone distributions in the North
1095 Atlantic and Nordic sea surface waters. Geochemistry, Geophysics, Geosystems,
1096 Article 2001GC000159.
1097 Sicre, M.-A., Labeyrie, L., Ezat, U., Duprat, J., Turon, J-L, Schmidt, S., Michel, E.,
1098 Mazaud A., 2005. Southern Indian Ocean response to Northern Hemisphere Heinrich
1099 events. Earth and Planetary Science Letters 240, 724-731, doi: 10.1016.
1100 Sicre, M.-A., Jacob, J., Ezat, U., Rousse, S., Kissel, C., Yiou, P., Eiriksson, J., Knudsen,
1101 K.-L., Jansen, E., Turon, J.-L., 2008a. Decadal variability of sea surface temperatures
1102 off North Iceland over the last 2000 years. Earth and Planetary Science Letters 268,
1103 137-142.
1104 Sicre, M-A., Yiou, P., Eiriksson, J., Ezat, U., Guimbaut, E., Dahhaoui, I., Knudsen, K.L.,
1105 Jansen, E., Turon, J.-L., 2008b. A 4500-year reconstruction of sea surface
1106 temperature variability at decadal time scales off North Iceland. Quaternary Science
1107 Reviews 27, 2041-2047.
1108 Simon, Q., Hillaire-Marcel, C., St-Onge, G., Andrews, J.T., 2014. North-eastern
1109 Laurentide, western Greenland and southern Innuitian ice stream dynamics during
1110 the last glacial cycle. Journal of Quaternary Science 29, 14-26.
1111 Skinner L.C. & I.N. McCave. Analysis and modelling of the behaviour of gravity and
1112 piston corers based on soil mechanical principles. Marine Geology 199, 181-204.
1113 Skinner, L. C., Muschitiello, F., & Scrivner, A. E., 2019. Marine reservoir age variability
1114 over the last deglaciation: Implications for marine carbon cycling and prospects for
1115 regional radiocarbon calibrations. Paleoceanography and Paleoclimatology 34,
1116 1807–1815. https://doi.org/10.1029/2019PA003667
1117 Stefansson, U., 1962. North Icelandic Waters. Rit Fiskideildar III. Bind, Vol 3, 269.
1118 Stein, R., 2008. Arctic Ocean Sediments. Processes, Proxies, and Paleoenvironment.
1119 Elsevier, New York.
1120 Stein, R., Nam, S.-I., Grobe, H., Hubberten, H., 1996a. Late Quaternary glacial history
1121 and short-term ice-rafted debris fluctuations along the East Greenland continental
1122 margin, in: Andrews, J.T., Austin, W.A., Bergsten, H., Jennings, A.E. (Eds.), Late

Quaternary paleoceanography of North Atlantic margins. Geological Society, London, pp. 135-151.

Stein, R., Nam, S.-Il., Grobe, H., Hubberten, Hans-Wolfgang, H., 1996b. Sedimentology and stable isotope ratios of cores from the East Greenland continental margin. *PANGAEA*, https://doi.org/10.1594/PANGAEA.733965,

Stokes, C.R., Clark, C.D., Darby, D.A., Hodgson, D.A., 2005. Late Pleistocene ice export events into the Arctic Ocean from the M'Clure Strait Ice Stream, Canadian Arctic Archipelago. Global and Planetary Change 49, 139-162.

Telford, R.J., Heegaard, E., Birks, H.J.B., 2003. All age-depth models are wrong: but how badly? Quaternary Science Reviews 23, 1-5.

Trachsel, M., Telford, R.J., 2017 All age-depth models are wrong, but are getting better. Holocene 27, 860-869 van Kreveld, S., Sarthein, M., Erlenkeuser, H.,

Grootes, P., Jung, S., Nadeau, M.J.,

Pflaumann, U., Voelker, A., 2000. Potential links between surging ice sheets, circulation changes, and the Dansgaard-Oeschger cycles in the Irminger Sea, 60-18 ka. Paleoceanography 15, 425-442.

Vasskog, K., Langebroek, P.M., Andrews, J.T., Nilsen, J.E.O., Nesje, A., 2015. The Greenland Ice Sheet during the last glacial cycle: Current ice loss and contribution to sea-level rise from a palaeoclimatic perspective. Earth-Science Reviews 150, 45-67.

Velay-Vitow, J., Peltier, W.R., and Stuhne, G. , 2019. Tides of the Glacial Ocean and their role in Heinrich Event instability. Geophysical Research Abstracts. 21, EGU2019-3733.

Venkatesh, S., Murphy, D.L., Wright, G.F., 1994. On the deterioration of icebergs in the marginal ice-zone. Atmosphere-Ocean 32, 469-484.

Verplanck, E.P., Farmer, G.L., Andrews, J., Dunhill, G., Millo, C., 2009. Provenance of Quaternary glacial and glacimarine sediments along the southeast Greenland margin. Earth and Planetary Science Letters 286, 52-62.

Voelker, A.H.L., 1999. Zur Deutung der Dansgaard-Oeschger Ereignisse in ultahochauflosenden Sedimentprofilen aus dem Europaischen Nordmeer, DansgaardOeschger events in ultra-high resolution sediment records from the Nordic Seas.

Universitat Kiel, Kiel, p. 271.

Voelker, A.H.L., Grootes, P.M., Nadeau, M-J., and Sarnthein, M., 2000. Radiocarbon levels in the Iceland Sea from 25–53 kyr and their link to the earth’s magnetic field intensity. Radiocarbon 42, p 437–452

Voelker, A.H.L., Haflidason, H., 2015. Refining the Icelandic tephrachronology of the last glacial period - The deep-sea core P52644 record from the southern Greenland Sea. Global and Planetary Change 131, 35-62.

Voelker, A.H.L., Sarnthein, M., Grootes, P.M., Erlenkeuser, H., Laj, C., ,Mazaud, A., Nadeau, M-J., Schleicher, M., 1998: Correlation of marine 14C ages from the Nordic Seas with the GISP2 isotope record: implications for 14C calibration beyond 25 ka BP. Radiocarbon 40, 517-534.

Volkman, J.K., 1986. A review of sterol markers for marine and terrigenous organic matter. Organic Geochemistry 9, 83–99.

Vogt, C., 2017. Bulk mineral assemblage via Quantitative Phase Analysis with X-ray diffraction of sediment core PS2644-5 KAL. PANGAEA. https://doi.org/10.1594/PANGAEA.875919

Walczuk, M.H. & 13 others, 2020. Phasing of millennial-scale climate variability in the Pacificand Atlantic oceans. Science, 370, 716–720.

Watkins, S.J., Maher, B.A., 2003. Magnetic characterization of present-day deep-sea sediments and sources in the North Atlantic. Earth and Planetary Science Letters 214, 379-394.

White, L.F., Bailey, I., Foster, G.L., Allen, G., Kelley, S.P., Andrews, J.T., Hogan, K., Dowdeswell, J.A., Storey, C.D., 2016. Tracking the provenance of Greenlandsourced, Holocene aged, individual sand-sized ice-rafted debris using the Pb-isotope compositions of feldspars and Ar-40/Ar-39 ages of hornblendes. Earth and Planetary Science Letters 433, 192-203.

Xiao, X., Fahl, K., Stein, R., 2013. Biomarker distributions in surface sediments from the Kara and Laptev seas (Arctic Ocean): indicators for organic-carbon sources and seaice coverage. Quaternary Science Reviews 79, 40–52.

Xiao, X., Zhao, M., Knudsen, K.L., Sha, L., Eiríksson, J., Gudmundsdóttir, E., Jiang, H., Guo, Z., 2017. Deglacial and Holocene sea–ice variability north of Iceland and response to ocean circulation changes. Earth and Planetary Science Letters 472, 14–24.

Zou, H., 2016. An X-Ray Diffraction Approach: Bulk Mineral Assemblages as Provenance Indicator of Sediments from the Arctic Ocean. University of Bremen, Bremen, pp. 116. https://elib.suub.uni-bremen.de/edocs/00105354-1.pdf.

Methods

Magnetic susceptibility: Magnetic susceptibility was measured on-board the *Marion Dufresne* (Labeyrie and Cort, 2005) in 2-cm increments (hence ~150yr sampling on average). Measurements were taken on the 1.5 m core sections. In this area of Iceland, the marine deposits are strongly affected by erosion and transport of basalt, which results in very high values of magnetic susceptibility. The export of sediments from the erosion of bedrock with much lower magnetic susceptibilities, such as granites and other felsicrich bedrock in NE Greenland and from more distant sources (Verplanck et al., 2009; White et al., 2016) will lower the magnetic susceptibility readings. It is important to note that although magnetic susceptibility is straightforward to measure, data interpretation is complex, being a product of sediment density, grain-size, and mineralogy (Robinson et al., 1995; Stoner and Andrews, 1999; Watkins and Maher, 2003).

Quantitative X-ray Diffraction (qXRD): The weight % (wt%) of the non-clay and clay mineral composition of the < 2 mm sediment fractions is based on the US

Geological Survey method (Eberl, 2003), which has been used extensively in this region (e.g. Andrews et al., 2017; Andrews and Eberl, 2007; Andrews and Vogt, 2014). One gram of sediment (dry weight) is spiked with 0.111 g of zincite, prepared (Eberl, 2003), run in the X-ray diffractometer, and the resulting intensity data processed in the Excel macro-program Rockjock v6. We investigate the wt% and presence/absence of 34 minerals and reduced this number by combining individual mineral wt% into larger groups, such as k-feldspars, plagioclase, dolomite, and amorphous minerals. Importantly in the context of this paper we had earlier shown that qXRD can recognize the presence of tephra and volcanic glass, with some ability to distinguish between basaltic and rhyolithic glass (Andrews et al., 2013).

To gain a better understanding of possible changes in the provenance of the mineral compositions we processed the mineral wt% data in a sediment unmixing program “SedUnMix” (Andrews and Eberl, 2012). Two models were considered, the first with qXRD results from #2274 with four appropriate bedrocks, namely: basalt, dolerite, gneiss, and granite; and secondly with the mineral compositions of glacial marine sediment samples from potential source areas, namely: NE Greenland, E. Greenland, and Iceland (Suppl. Table of bedrock and marine sediment sources). The program calculates a “degree of fit” and also derives error estimates on each source within a sample. Ideally, the sum of the sources should equal 100% but marked deviations from this suggest that one or more sources have not been included, and/or that the sources are not representative of the sediment samples.

Grain-size: Sediment was wet-sieved at 2 mm and the grain-size volume percentages in 96 intervals between 0.01 and 2000 µm were obtained via a Malvern laser

system. Comparisons between the Malvern and other grain-size systems have been documented and found comparable (McCave et al., 2006; McCave and Syvitski, 1991). However, the objections of McCave et al. (2006) to laser sizers on the grounds of grain shape (Konert and Vandenberghe, 1997) are not valid for equant grains such as those produced by glacial grinding, as pointed out by Piper (Marshall et al., 2014), and thus size data are believed valid in the setting of MD2274. Grain-size curves have provided vital information on sediment transport and deposition in this region, and methods have been developed to reconstruct variations in bottom current speed for sediments delivered to the ocean from dominantly glacial sources (McCave and Andrews, 2019a, b) The calibration of sortable silt mean (mean of 10-63 μm), a sensitivity, by McCave et al.,(2017) has been applied to changes in the grainsize record.

Biomarkers: Biomarkers were extracted from freeze-dried subsamples (~2-4 g). Prior to extraction, samples were spiked with an internal standard (9-octylheptadec-8-ene, 9-OHD, 10 μL; 10 μg mL^{-1}) to permit quantification of the highly branched isoprenoid (HBI) biomarkers IP_{25}, HBI II and HBI III. 5α-androstan-3β-ol; (0.1 μg) was also added to permit quantification of brassicasterol in some cases. Samples were then saponified in a methanolic KOH solution (~5 mL H_2O:MeOH (1:9); 5% KOH) for 60 min (70 °C). Hexane (3×2 mL) was added to the saponified mixtures, with supernatant solutions, containing non-saponifiable lipids (NSLs), transferred by glass pipettes to glass vials, and solvent removed using a gentle stream of N_2. Dried NSLs were re-suspended in hexane (0.5 mL) and fractionated using column chromatography (SiO_2; 0.5 g). Non-polar lipids, including IP_{25} and HBI II, were eluted with hexane (6 mL), while more polar lipid fractions containing alkenones were eluted with MeOH (6 mL). For a few horizons,

additional NSLs were fractionated to yield non-polar (hexane; 6 mL) and polar fractions containing sterols (hexane:methyl acetate 4:1; 6 mL). Each non-polar fraction was further purified to remove saturated components using silver-ion chromatography (Belt et al., 2015), with saturated compounds eluted with hexane (2 mL) and unsaturated compounds, including IP_{25} and other HBIs, collected in a subsequent acetone fraction (3 mL). Analysis of fractions containing IP_{25} and other HBIs was carried out using gas chromatography–mass spectrometry (GC–MS) following the methods and operating conditions described prevously (Belt et al., 2012). Mass spectrometric analysis was carried out in total ion current (TIC) and selected ion monitoring (SIM) modes. The identification of IP_{25} and HBI II was based on their characteristic GC retention indices (e.g. RI_{HP5MS} = 2081,2082 and 2044 for IP_{25}, HBI II and HBI III, respectively) and mass spectra (Belt, 2018). Quantification of all HBIs was achieved by comparison of mass spectral responses of selected ions (e.g. IP_{25}, *m/z* 350; HBI II, *m/z* 348; HBI III, *m/z* 346) in SIM mode with those of the internal standard (9-OHD, *m/z* 350) and normalized according to their respective instrumental response factors, derived from solutions of known biomarker concentration, and sediment masses (Belt et al., 2012). Fractions containing sterols were derivatized with N,O-bis(trimethylsilyl)trifluoroacetamide (BSTFA; 100 µL; 70°C for 60 min) immediately prior to analysis by GC–MS. Sterols were identified by comparison with GC–MS responses compared to those of standards. Sterol quantification was achieved as per the approach described above for HBIs.

Polar factions containing alkenones obtained from elution with MeOH (6 mL) were further purified with 2 mL of hexane:methyl acetate (95:5 v/v) and 2 mL of hexane:methyl acetate (90:10 v/v). Alkenones were analyzed using a Thermo Trace GC Ultra gas

chromatograph equipped with a CPSil5 capillary column (50m length, 0.32 i.d. and 0.25 mm film thickness), an FID detector and a septum programmable injector (SPI). Helium was used as carrier gas. 5a-cholestane was added as an external standard prior to GC injection. SST estimates were determined using the following equation (Prahl et al., 1988).

$$K'_{U37} = \frac{C_{37:2}}{C_{37:2} + C_{37:3}} = 0.034\ T + 0.039$$

References

Andrews, J.T., Dunhill, G., Vogt, C., Voelker, A.H.L., 2017. Denmark Strait during the Late Glacial Maximum and Marine Isotope Stage 3: Sediment sources and transport processes. Marine Geology 390, 181-198.

Andrews, J.T., Eberl, D.D., 2007. Quantitative mineralogy of surface sediments on the Iceland shelf, and application to down-core studies of Holocene ice-rafted sediments. Journal of Sedimentary Research 77, 469-479.

Andrews, J.T., Eberl, D.D., 2012. Determination of sediment provenance by unmixing the mineralogy of source-area sediments: The "SedUnMix" program. Marine Geology 291, 24-33.

Andrews, J.T., Vogt, C., 2020. Variations in felsic- versus mafic-sources in the Western Nordic Seas during MIS 1 to MIS 4 Marine Geology 424, 106164.

Belt, S.T., 2018. Source-specific biomarkers as proxies for Arctic and Antarctic sea ice, Organic Geochemistry 125, 277–298, doi: 10.1016/j.orggeochem.2018.10.002.

Belt, S.T., Brown, T.A., Navarro-Rodriguez, A., Cabedo-Sanz, P., Tonkin, A., Ingle, R., 2012. A reproducible method for the extraction, identification and quantification of the Arctic sea ice proxy IP_{25} from marine sediments. Analytical Methods 4, 705–713.

Belt, S.T., Cabedo-Sanz, P., Smik, L., Navarro-Rodriguez, A., Berben, S.M. P., Knies, J., Husum, K., 2015. Identification of paleo Arctic winter sea ice limits and the marginal ice zone: optimised biomarker-based reconstructions of late Quaternary Arctic sea ice. Earth and Planetary Science Letters 431, 127-139.

Eberl, D.D., 2003. User guide to RockJock: A program for determining quantitative mineralogy from X-ray diffraction data. United States Geological Survey, Open File Report 03-78, 40 pp, Washington, DC.

Konert, M., Vandenberghe, J., 1997. Comparison of laser grain size analysis with pipette and sieve analysis: a solution for the underestimation of the clay fraction. Sedimentology 44, 523-535.

Marshall, N.R., Piper, D.J.W., Saint-Ange, F., Campbell, D.C., 2014. Late Quaternary history of contourite drifts and variations in Labrador Current flow, Flemish Pass, offshore eastern Canada. Geology Marine Letters 34, 457-470. doi:10.1007/s00367014-0377-z.

McCave, I.N., Andrews, J.T., 2019a. Distinguishing current effects in sediments delivered to the ocean by ice. I. Principles, methods and examples. Quaternary Science Reviews 212, 92-107.

McCave, I.N., Andrews, J.T., 2019b. Distinguishing current effects in sediments delivered to the ocean by ice. II. Glacial to Holocene changes in North Atlantic high latitude upper ocean flows. Quaternary Science Reviews 223, no. 105902, 21pp.

McCave, I.N., Hall, I.R., Bianchi, G.G., 2006. Laser vs settling velocity differences in silt grainsize measurements: estimation of palaeocurrent vigour. Sedimentology 53, 919928.

McCave, I.N., Manighetti, B. and Robinson, S.G., 1995. Sortable silt and fine sediment size/composition slicing: parameters for palaeocurrent speed and palaeoceanography. Paleoceanography 10, 593-610.

McCave, I.N., Thornalley, D.J.R., Hall, I.R., 2017. Relation of sortable silt grain-size to deep-sea current speeds: Calibration of the 'Mud Current Meter'. Deep-Sea Research Part I 127, 1-12.

McCave, I.N., Syvitski, J.P.M, 1991. Principles and methods of geological particle size analysis, in: Syvitski, J.P.M. (Ed.), Principles, methods and application of particle size analysis. Cambridge University Press, pp. 3-21.

Robinson, S.G., Maslin, M.A., McCave, I.N., 1995. Magnetic susceptibility variations in Upper Pleistocene deep-sea sediments of the N.E. Atlantic: Implications for ice rafting and palaeocirculation at the Last Glacial Maximum. Paleoceanography 10, 221-250.

Stoner, J.S., Andrews, J.T., 1999. The North Atlantic as a Quaternary magnetic archive, in: Maher, B., Thompson, R. (Eds.), Quaternary Climates, Environments and Magnetism. Cambridge University Press, Cambridge, UK, pp. 49-80.

Verplanck, E.P., Farmer, G.L., Andrews, J., Dunhill, G., Millo, C., 2009. Provenance of Quaternary glacial and glacimarine sediments along the southeast Greenland margin. Earth and Planetary Science Letters 286, 52-62.

Watkins, S.J., Maher, B.A., 2003. Magnetic characterization of present-day deep-sea sediments and sources in the North Atlantic. Earth and Planetary Science Letters 214, 379-394.

White, L.F., Bailey, I., Foster, G.L., Allen, G., Kelley, S.P., Andrews, J.T., Hogan, K., Dowdeswell, J.A., Storey, C.D., 2016. Tracking the provenance of Greenlandsourced, Holocene aged, individual sand-sized ice-rafted debris using the Pb-isotope compositions of feldspars and Ar-40/Ar-39 ages of hornblendes. Earth and Planetary Science Letters 433, 192-203.

Figure

Click here to access/download;Figure;THIS Fig. 1A,B,C Oct.tif

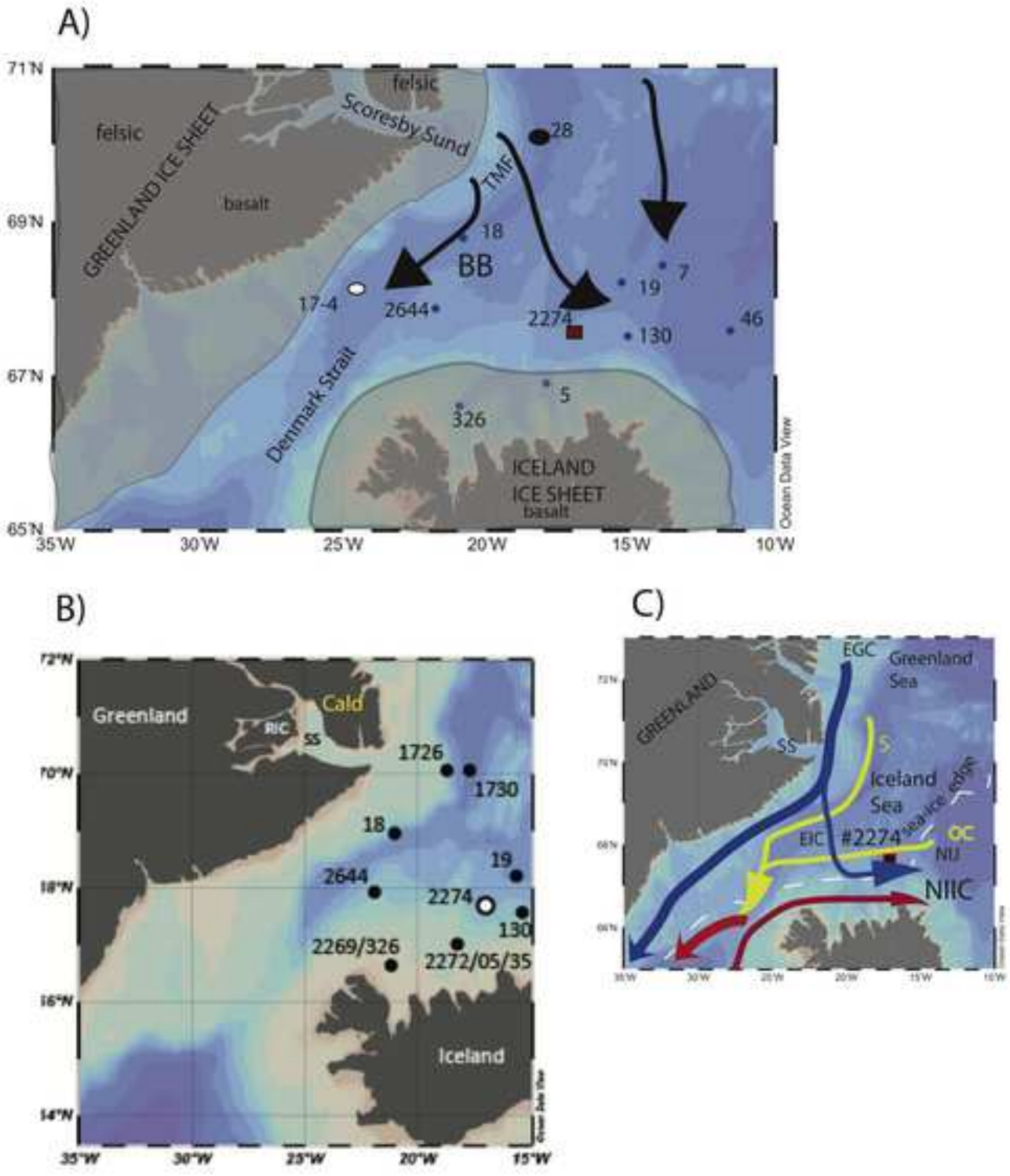

Figure

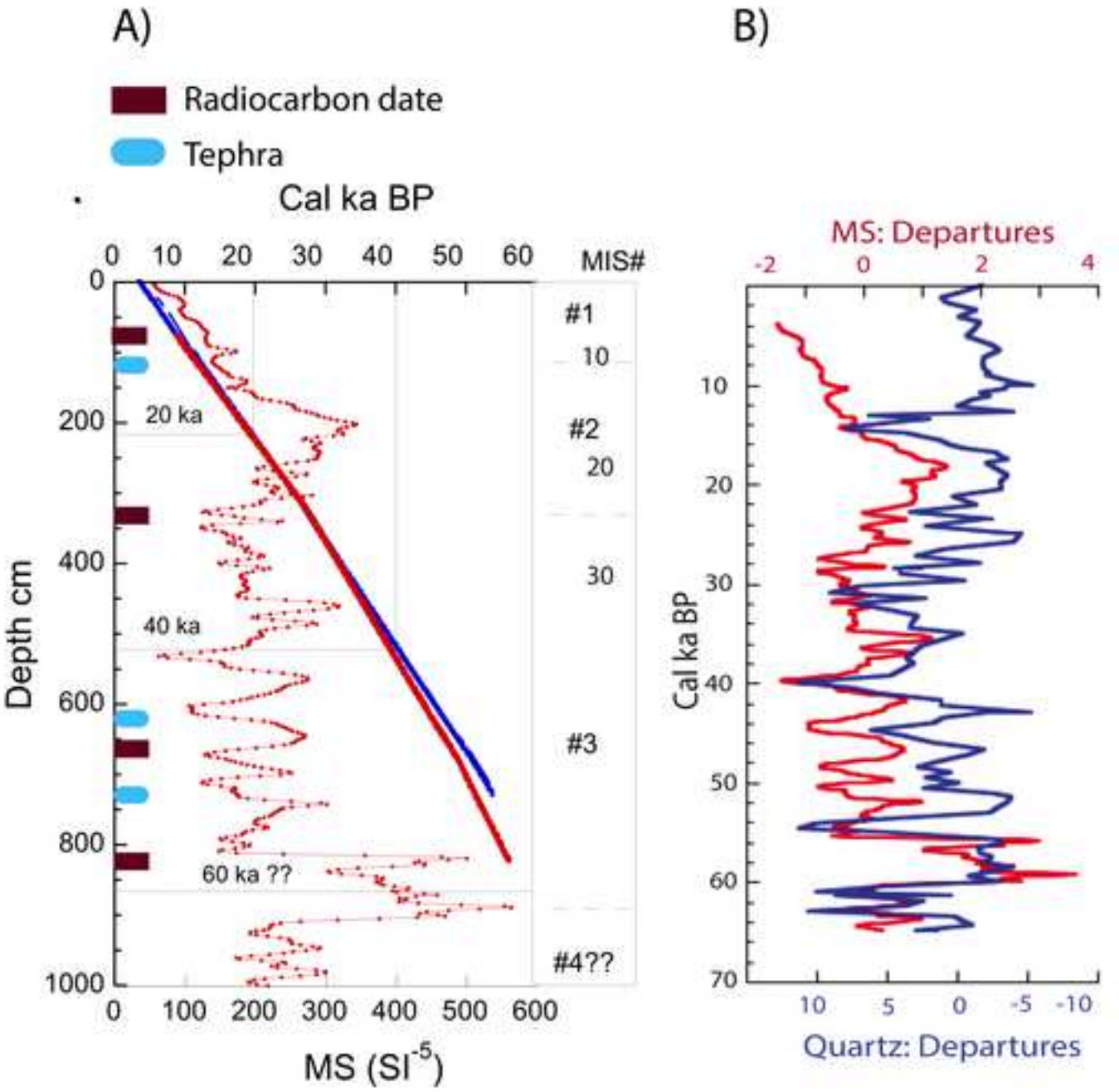

Figure

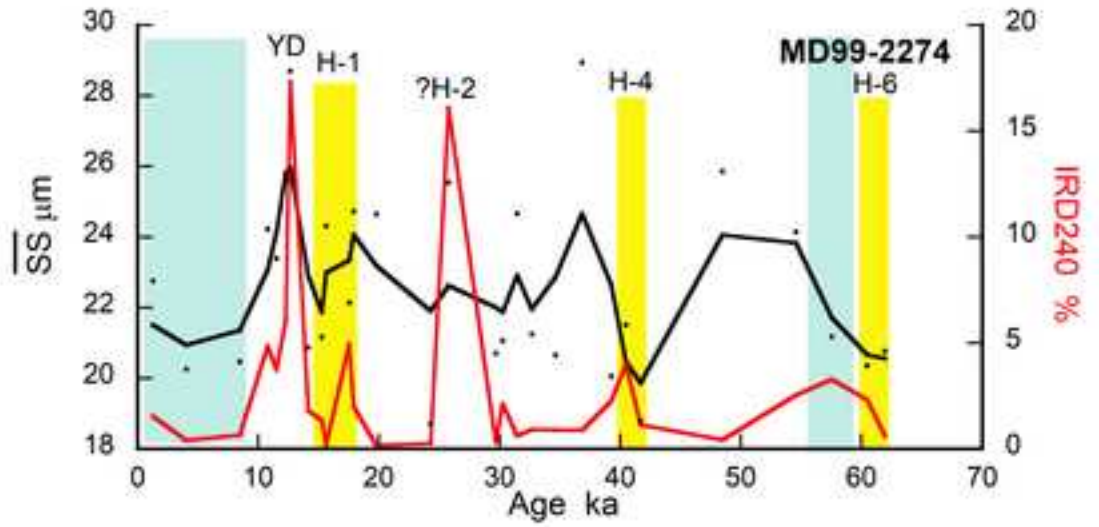

Figure

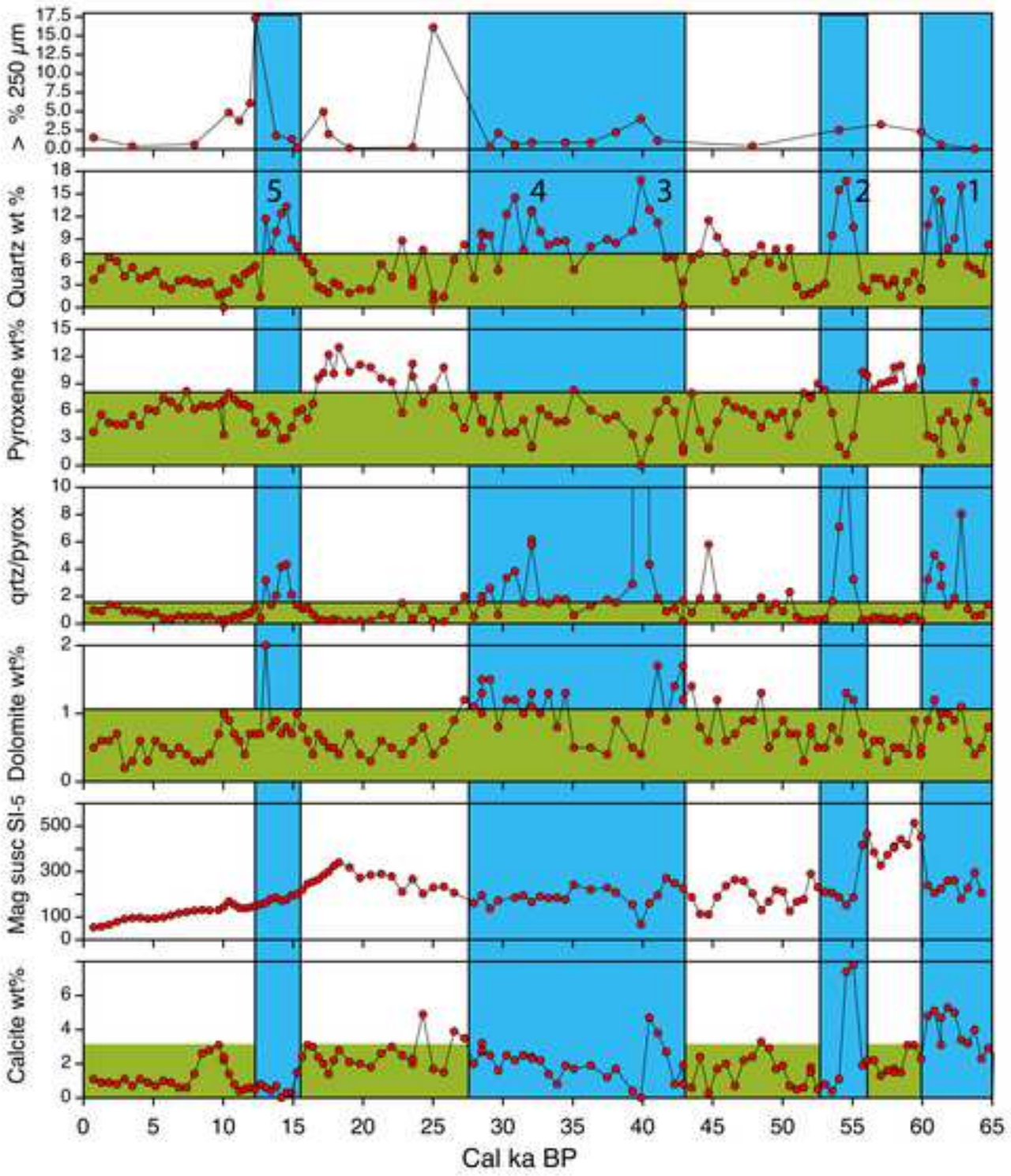

Figure

Click here to access/download;Figure;Fig. 5 August.tif

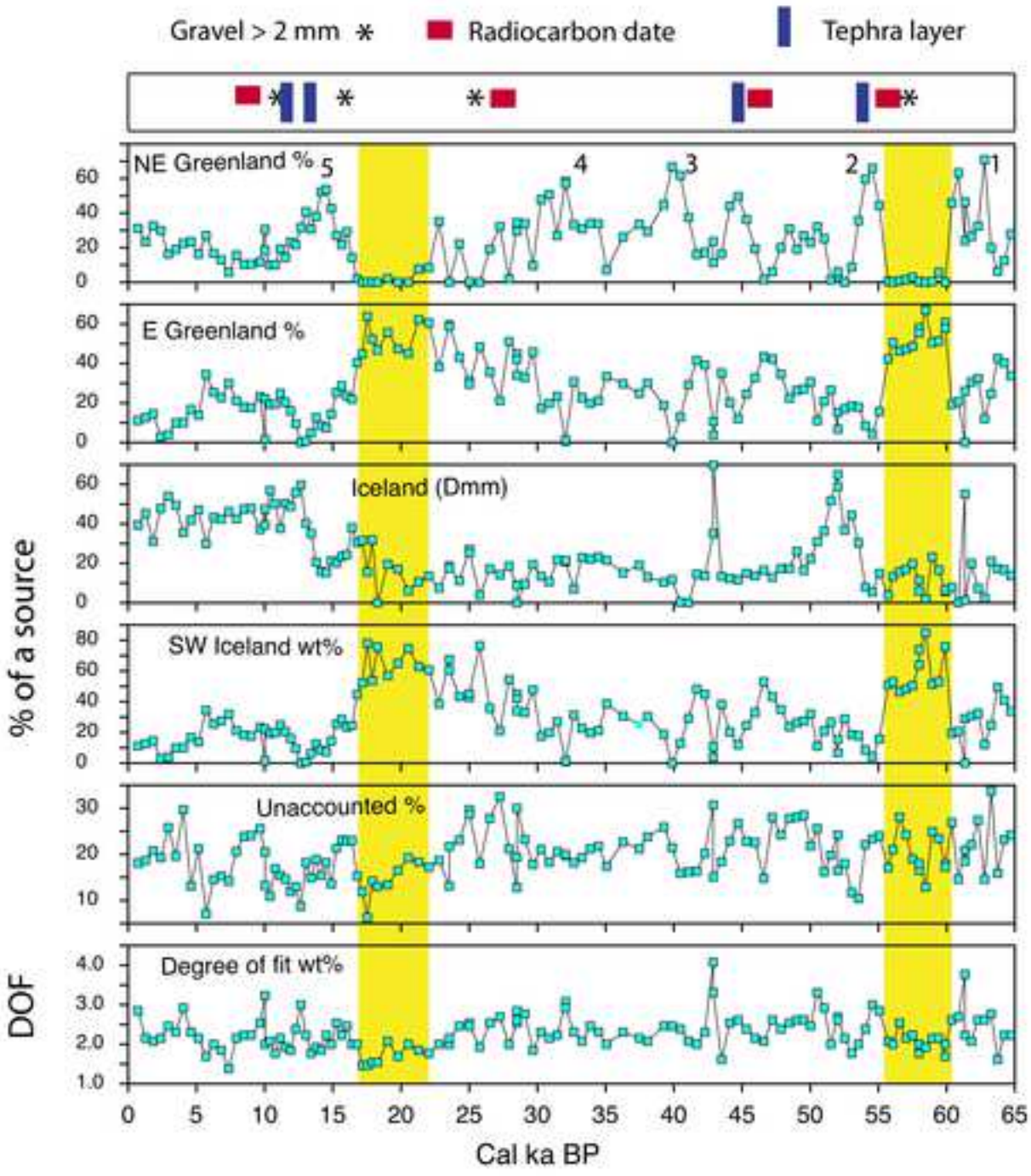

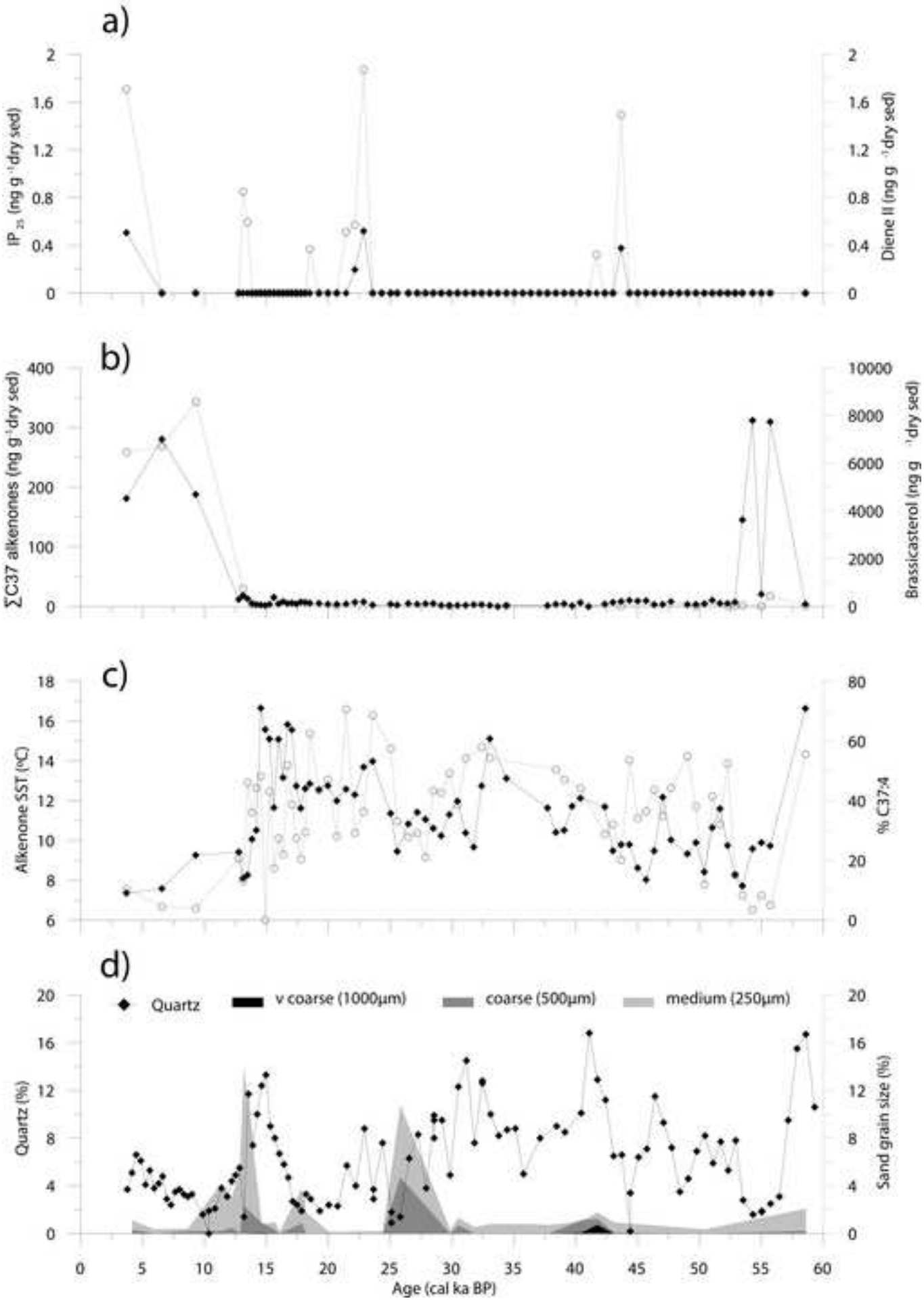

Figure

Click here to access/download;Figure;Fig. 7 August summary .tif